MASTERARBEIT / MASTER'S THESIS

Titel der Masterarbeit / Title of the Master's Thesis

„Hydrotectonics of the Eisensteinhöhle"

verfasst von / submitted by

Jonas Hardege BSc

angestrebter akademischer Grad / in partial fulfilment of the requirements for the degree of

Master of Science MSc

Wien, 2018 / Vienna 2018

Studienkennzahl lt. Studienblatt / degree programme code as it appears on the student record sheet:	A 066 815
Studienrichtung lt. Studienblatt / degree programme as it appears on the student record sheet:	Erdwissenschaften
Betreut von / Supervisor:	Univ.-Prof. Mag. Dr. Bernhard Grasemann
Mitbetreut von / Co-Supervisor:	Mag. Dr. Lukas Plan

Table of contents

Acknowledgments

First and foremost, I would like to thank my supervisors Lukas Plan and Bernhard Grasemann, for their support through all stages of this thesis and also for their encouragement to present this research to the scientific community. Special thanks go to Lukas Plan, for introducing me into the fields of speleology and karst science and whose discussions, comments and remarks were inevitable through the process of learning and writing.

Furthermore, I would like to thank Ivo Baron, Rudolf Pavuza and Michi Nagl for their support during fieldwork and especially Gerhard Winkler for sharing the notes, he took over the last 25 years.

For their help with the pumping test I'd like to thank Dieter Sulzbacher and Alexandra Haslauer.

Thanks go to Mag. Friedrich Salzer and Kurt Luger (both Government of Lower Austria) for providing hydrological data and to Wolfgang Lenhard (ZAMG) for answering several requests for updates of the Earthquake Catalogue.

Last but not least, I would like to thank my colleagues, friends and family for their support. Klemens for sharing his MATLAB skills and David, Cornelius and Pedro for inspiring and entertaining discussions. Sincere thanks go to my family that supports me in every sense and to Anna who always encouraged me when my motivation subsided.

List of Figures and Tables

Abstract

The cave Eisensteinhöhle is a 2-km long crevice cave that is significantly overprinted by hydrothermal karst processes. It was opened during quarrying in the Fischau Hills, on the western margin of the Vienna Basin. This pull-apart basin cuts the eastern foothills of the Alps and is formed by a major NE-SW striking, sinistral transform fault. The western margin consists of NNE-SSW striking normal faults that create paths for thermal water to rise from the central basin.

The deepest part of the cave, 73 m below the entrance, hosts a pond with 15.5 +/- 0.4 °C warm water, that sometimes acts as a spring. The cave and in particular the spring have attracted attention since their discovery in 1855. The water level and temperature fluctuate and at a certain level, water visibly discharges into a nearby narrow fissure. A record of sporadically taken data on water level and discharge exists from the late 1980s on. As there was no obvious connection to precipitation events or periods, it was impossible to determine how the spring is connected to an aquifer and where the water comes from.

Gerhard Winkler, a local cave guide, began systematic observations with the installation of a stick gauge in 1992 and took measurements whenever he visited the cave. In October 2015, a data logger (SEBA Dipper PT) was installed for automated measurements of the water level and temperature of the spring.

A pumping test, conducted on 13/7/2016, showed the geometry and the volume of the spring of about 2.8 m^3 and that it is fed by a very small inlet out of the sandy bottom. At the time of the pumping test, the discharge was only 4.5 l/h but during previous overflow events, discharges of up to 289 l/h were recorded.

Water temperature and hydrochemistry hint towards a mixture of an old thermal component and a young meteoric component. Within the first two years of the continuous monitoring, the water level was almost stable with few periods of high level (almost at overflow) that lasted for about 3 to 4 weeks each. The water temperature increased during most water high stands and is positively correlated with the water level. Correlation of the high-resolution data on water level and temperature fluctuations with precipitation measurements at the nearest meteorological stations show a relation of water level to certain rainfall events and the sporadically taken long time records show a correlation with annual precipitation sums. Long-term observations also indicate a connection to groundwater levels in the Vienna Basin with a delay of water level changes of about 8 weeks in Bad Fischau.

In July 2017, the water level dropped suddenly and then recovered simultaneously to several weak earthquakes in the vicinity.

The collected data suggests that the spring in Eisensteinhöhle is influenced by both, precipitation and tectonics, but a lack of tectonic events leaves this relation unconfirmed.

Zusammenfassung

Die Eisensteinhöhle ist eine etwa 2 km lange Spalthöhle, deren Morphologie bedeutend von hydrothermalen Karstprozessen überprägt wurde. Sie wurde 1855 während Steinbrucharbeiten in den Fischauer Bergen am Westrand des Wiener Beckens angefahren. Während sich das Wiener Becken im Miozän entlang SW-NE streichender Blattverschiebungen öffnete, bilden SSW-NNE streichende Abschiebungen den Abbruch Nördlichen Kalkalpen zum Beckeninneren.

Im tiefsten Abschnitt der Höhle, 73 m unterhalb des Eingangs liegt ein, meist mit Wasser gefüllter Quellsiphon mit auffällig schwankendem Wasserstand, der ab einem Niveau von -71,8 m in den nebenliegenden Raum abläuft. Insbesondere die Quelle weckte aufgrund der schwankenden Schüttungsrate und der mit ca. 15 +/- 0.5 °C, im Vergleich zu normalem Grundwasser, leicht erhöhten Temperatur immer wieder Interesse.

Gerhard Winkler, ein Höhlenführer begann bereits 1968 seine Beobachtungen über die Quelle aufzuschreiben. Da kein offensichtlicher Zusammenhang der Schüttungsschwankungen zu Niederschlägen bestand baute er 1992 eine Messlatte ein um genauere und systematischere Messungen vornehmen zu können.

Die 23 Jahre lange Messreihe wurde ergänzt durch Pegel- und Temperaturmessungen die von Oktober 2015 bis November 2017 mit einem automatischen Datenlogger (SEBA Dipper PT) durchgeführt wurden.

Bei einem einfachen Pumpversuch, am 13.7.2016, konnte die Form des wassergefüllten Hohlraumes vermessen und dessen Volumen bestimmt werden. Während des Pumpversuchs konnte eine Schüttung von lediglich 4.5 l/h gemessen werden, frühere Messungen ergaben Werte bis zu 289 l/h.

Während der 2 Jahre in denen automatische Messungen durchgeführt wurden, lag der Wasserstand relativ konstant bei 307,0 m ü.A. mit Ausnahme einiger Perioden in denen der Pegel fast den Überlauf erreichte. Diese Phasen dauerten je 3-4 Wochen an. Die Wassertemperatur stieg parallel dazu mit einer Verzögerung von einigen Tagen. Die Korrelation der hoch-aufgelösten Pegelmessungen mit Niederschlagsmessungen der umliegenden Wetterstationen zeigt einen Zusammenhang zwischen der Schüttung und starken Einzelniederschlägen, die Langzeitbeobachtungen deuten jedoch auch auf einen Zusammenhang mit der jährlichen Niederschlagssumme hin. Durch die Langzeitbeobachtungen konnte auch eine klare Verbindung der Quelle mit dem Grundwasser

im Wiener Becken nachgewiesen werden, wo an einem Pegel in Bad Fischau Schwankungen mit einer Verzögerung von 8 Wochen aufgezeichnet werden.

Erste Hinweise auf eine Beeinflussung der Quellschüttung durch tektonische Prozesse konnten in Juli und August 2017 gesammelt werden, als ein plötzliches Absinken des Pegels in der Eisensteinhöhle, gefolgt von einem Anstieg auf das vorherige Niveau zeitgleich mit mehreren schwachen Erdbeben in der Nähe, gemessen wurde.

Die gesammelten Daten legen nahe, dass die Thermalquelle in der Eisensteinhöhle sowohl durch Niederschlag als auch durch aktive Tektonik beeinflusst wird. Durch die geringe Anzahl an Erdbeben bleibt dieser Zusammenhang jedoch statistisch nicht aussagekräftig belegt.

1. Introduction

To the south of Vienna, a zone of numerous faults forms the margin of the Vienna Basin (VB). Thermal water uses the fault systems, which accounts for the steep drop of the alpine units towards the centre of the basin, as a pathway through layers of impermeable sediments (Wessely, 1983). On the surface, it discharges from several lukewarm springs.

The southernmost thermal spring at the western margin of the VB is a spring with fluctuating discharge in the deepest part of the 2 km long show cave Eisensteinhöhle (EISE). EISE is a crevice cave with in some parts significant overprint by hypogene karst processes.

The spring fills a pond that rarely overflows into a neighbouring gallery through a fissure. This particular discharge behaviour lead Gerhard Winkler, a local speleologist and guide for tours into the cave, to make sporadic observations from 1968 on (Winkler, 1992). To have a more accurate record on the water level he installed a stick gauge in 1992 and since then he took measurements during every visit to the cave.

Recently, evidence of active tectonics was found while monitoring fault activity by measuring the fault displacement inside EISE and Emmerberghöhle (a 135 m-long cave, 3.5 km SW of EISE) with an opto-mechanical 3D crack gauge (Baroň et al., 2016). In November and December 2013, displacement was recorded in both caves prior to a Magnitude 3 earthquake in Bad Fischau.

Within more than 30 years of sporadic observations no clear link between the water level (including the rare overflows) at EISE and precipitation at nearby meteorological stations could be established. Now the latest findings lead to the question if the discharge behaviour could be influenced by active tectonics. Active tectonics and earthquakes have an influence on the environment in many ways including effects on groundwater that range from liquefaction and mud volcanoes to changes in groundwater levels, temperature and composition (e.g. Wang and Manga, 2010).

The aim of this study is to observe the factors influencing the hydrothermal spring in EISE and to find out if tectonic activity plays a role. This was done by analysis and evaluation of sporadic long-term observations, combined with hourly data on water level and temperature from October 2015 to November 2017. For a better understanding of the connection of the spring to an aquifer, a pumping test was performed. Furthermore, for an insight into the possibly influencing factors, hydrologic data and the Austrian Earthquake Catalogue were analysed

1.1. Hydrothermal spring in Eisensteinhöhle

The thermal springs in the VB have been used as spas by the Romans already 2000 years ago (Zötl, 1997). The spa around the lukewarm springs (19 °C) in Bad Fischau was built in 1872 and in Brunn an der Schneebergbahn an ephemeral pond, filled by two lukewarm springs (up to 23 °C C°) is used as a bath.

EISE caused interest in researchers since it was opened and from its deepest parts the Austrian poet F.J. Leitner described a water flow causing *a mumbling, ripple and swoosh* in 1909 (Winkler, 1992). The thermal spring that caused these sounds was then found in 1919 when a new gallery was opened by a blast (Winkler, 1992).

Most of the time, this spring is recognised as a pool with fluctuating water level that discharges through a crack into the neighbouring gallery only during high water. Due to its peculiar discharge behaviour, it attracted attention since its discovery. It has been described as a *perennial trickle* (german: *perennierender Riesel;* Mühlhofer, 1932) and a *thermal spring of very poor quality and quantity* (Hock, 1948). Pirker (1951) described it as a *small spring with strongly fluctuating discharge*, but neither the hydrothermal origin nor the reason for the discharge fluctuations could be explained.

Observations by the cave guide Gerhard Winkler described erratic water level fluctuations and rare overflows until the spring ran dry in 1971 (Winkler, 1992). Excavations of mud at the bottom of the spring reached the water table 1.8 m below its initial level before it dropped even further. In 1979, the spring started running again and settled to a new, in average lower water level. Nevertheless, the peculiar water level fluctuations continued and occasionally, during high discharge when the water level reached the overflow, a discharge of up to 240 l/h was measured (Winkler, 1992).

1.2. Hydrotectonics, earthquake-induced hydrological phenomena and hydrodynamic earthquake precursors

Earthquakes cause a variety of effects. The best known are probably ground shaking and related damage to buildings (e.g. Grünthal et al., 1998). Less familiar are effects on the environment, which are listed in the Environmental Seismic Intensity Scale (Michetti et al., 2007). Besides rock fall, Tsunami waves and surface ruptures, also effects on ground- and surface waters are known. Water level changes, variations in spring discharge or pore pressure in aquifers and changes of chemical and physical properties like the amount of dissolved solids, temperature and turbidity are outlined by the term earthquake-induced hydrological phenomena (Muir-Wood and King, 1993; Rojstaczer et al., 1995; Roeloffs, 1996; Wang and Manga, 2010).

Earthquake-induced hydrological phenomena can appear in many ways and can be observed up to several hundred (sometimes thousand) kilometres from the earthquake's epicentre. They play an important role in estimating the intensity of earthquakes (Michetti et al., 2007) and can provide an insight into local tectonics and earthquake generating processes (Roeloffs, 1988).

Variations in spring discharge and the emergence of new springs seem to be related to groundwater that was stored in the catchment and released due to increased permeability caused by the earthquake (Wang and Manga, 2015). Changes in ground water levels can appear as step-like, coseismic changes in the near field of the ruptured fault (distances of about the rupture length of the earthquake causing fault), as more gradual changes that last over several days or weeks in the intermediate field or as water level oscillations in the far field (distances of many ruptured fault lengths; Wang and Manga, 2010).

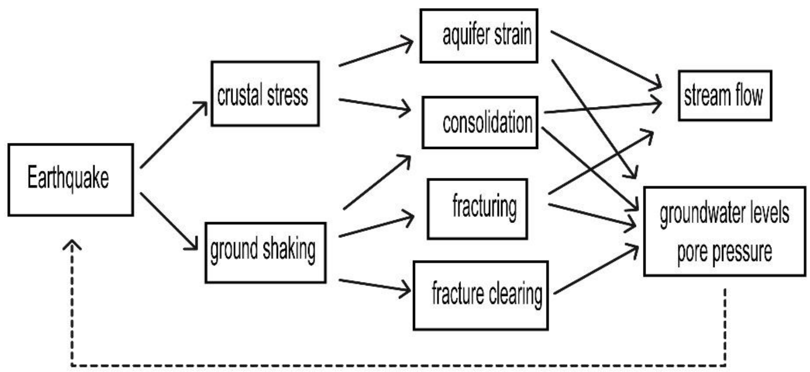

Figure 1: Flow model of interaction of earthquakes and hydrogeology (from Montgomery and Manga, 2003).

Several different mechanisms, underlying variations of groundwater levels have been proposed:

One mechanism in the near field is the enhancement of permeability mentioned above. This is caused by mobilisation of colloidal particles in porous aquifer and by unblocking fractures through shaking of the seismic waves (see Figure 1). Also increasing the permeability is the opening of fractures due to coseismic static strain (Rojstaczer et al., 1995).

Another mechanism for changes in groundwater levels is the shaking-induced consolidation of younger sediments (e.g. alluvial fans or basin sediments), where a volumetric decrease leads to an increase of pore pressure and therefore to a rising water level (Wang et al., 2001).

On the other hand, the earthquake-induced static strain can change aquifer properties depending on the relative location to the epicentre. In regions of compressive strain, water levels tend to increase during earthquakes while they show a water level decrease in dilatational settings (see

Figure 2; Lai et al., 2016). According to Larsson (1972) who studied the influence of the tectonic regime on fractured aquifers in granites of the Baltic Shield, shear faults are supposed to be tight with low permeability, while tension faults are open and have a high permeability. This is supposed to be valid for fractured rock aquifers.

In the far field water level, oscillations in wells coincide with the ground motion that is generated by earthquakes (Brodsky, 2003). Depending on well properties and aquifer characteristics, they can be used as hydroseismograms (Cooper et al.,1965; Wang and Manga 2010).

All earthquake-induced changes in spring discharge and groundwater levels are related to the seismic energy density (Figure 3), which is a function of earthquake magnitude and distance of the observed site to the epicentre (Montgomery and Manga, 2003). A certain threshold of energy must be reached to induce hydrological effects, which in turn means that the hydrological effects can occur only within a certain distance.

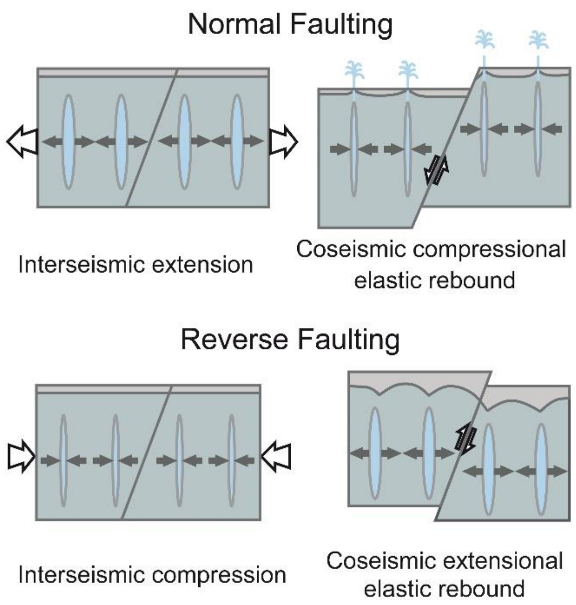

Figure 2: Elastic rebound model (after Wang and Chia, 2008).

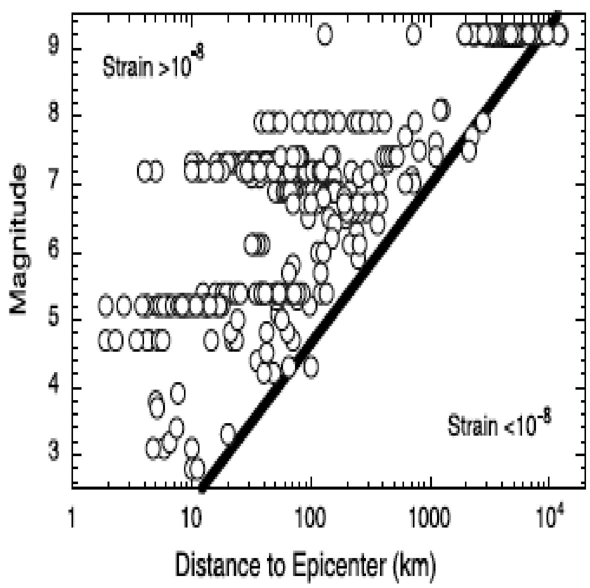

Figure 3: Relation between earthquake magnitude and distance of well from the epicentre for observed earthquake-induced groundwater level changes and variations in spring discharge (from Montgomery and Manga, 2003). The strain corresponds to seismic energy density.

Coseismic temperature changes in thermal springs are related to the increase of permeability of fractures (Mogi et al., 1989) enhancing water flow from the heat source to the spring, while temperature changes in wells may often be caused by the turbulent mixing of stratified water (Shi et al., 2007).

Hydrologic phenomena can also occur before earthquakes (i.e. precursor phenomena). As a reaction of aquifers to crustal strain, they are potential tools for earthquake prediction. However, their variability and the difficulties to distinguish them from other influencing factors (like precipitation, snowmelt or barometric influences) limit their application (Roeloffs, 1988; Wyss and Jackson, 1997).

2. Study site

The location of EISE is coined by the transition from the margin of the Northern Calcareous Alps with the Hohe Wand and the Fischau Hills to the plains of the southern VB (Figure 4).

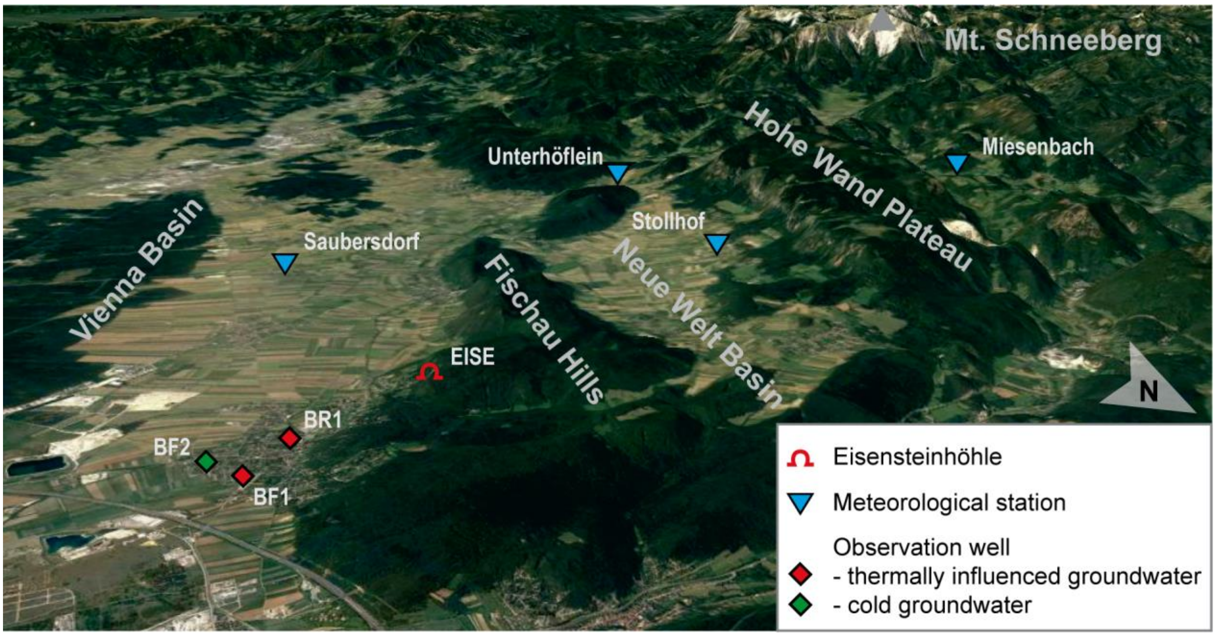

Figure 4: View from NE over the study area with all observation points. On the lower end, the frame covers about 8 km. The relief is displayed with 1.5 times vertical exaggeration. (Map data: Google, Landsat and DigitalGlobe).

2.1. Geographic setting

The Hohe Wand is a rugged, mountainous karst plateau with elevations up to 1134 m a.s.l. A steep cliff cuts of the plateau towards the Neue Welt Basin (NWB) in the southeast. To the east, the NWB is confined by the Fischau Hills, a ridge with elevation of up to 605 m a.s.l. marking the western margin of the southern Vienna Basin and dividing it from the NWB.

The climate in the study area is rather dry with annual precipitation between 770 mm/a at Hohe Wand and 599 mm/a at Wiener Neustadt (ZAMG, 2018) and a mean temperature of around 9 °C. Even though the precipitation maximum is during summer, due to lower evapotranspiration the main period of groundwater recharge is during the winter months (Fenzl, 1977).

2.2. Geological setting

2.2.1. Regional stratigraphy

Around the study site, several lithological units from Triassic to Neogene age are exposed as well as Quaternary sediments (Figure 5).

The oldest rocks are Triassic carbonates, the Hallstätter Kalk, Wandriffkalk and Wettersteinkalk and -dolomit. They form the Hohe Wand Plateau and the ridge of the Fischau Hillsas well as the basement of both, the VB and the NWB.

The limestones are well karstified and several caves, dolines and karren occur on Hohe Wand and Fischau Hills. In the latter, the morphology of many caves indicates a hydrothermal origin (Spötl et al., 2018).

Overlying the Triassic carbonates, sedimentary rocks of the Cretaceous Gosau Group follow on a transgressive contact and make up the filling of the NWB and a graben-like structure on the Fischau Hills. These are mostly clastic sediments with a basal breccia and conglomerate containing clasts of carbonate, quartz and chert and later following sandstone and claystone.

On the eastern slope of the Fischau Hills Neogene sediments crop out. Particularly interesting is the so-called Wurstmarmor (translated as *Sausage Marble*; named after the resemblance of coarse bright clasts in reddish matrix), a carbonate breccia of arguable stratigraphic classification. Plöchinger (1967) suggests, that it was deposited during the Lower Badenian, about 16 million years ago in a coastal, marine environment as one of the oldest sediments in the VB and considers it a variety of the Gainfarner Brekkzie. It is generally poorly sorted in terms of mineralogy, size and shape of its clasts. Clasts sizes vary from few millimetres to several centimetres and are sub-angular to rounded.

While most clasts consist mainly of limestone, dolomite and marine fossils, some clasts are also composed of silicate minerals and Cretaceous Gosau-sediments. The matrix is a reddish micrite. The mineralogy of the grains points towards a source area in the Northern Calcareous Alps that formed the hinterland during sedimentation.

Overlying the Wurstmarmor, the Badener Konglomerat, a grey conglomerate with rounded clasts of light grey carbonate with grain sizes of few millimetres, followed by the Brunner Konglomerat.

The cave is situated in the transition zone from the tectonic regions of the NCA to the VB. While the exposed Triassic carbonates of Hohe Wand Plateau and Fischau Hills belong to the Hohe Wand Nappe, that is part of the Mürzalpen Nappe System, the Neogene units are basin sediments (Plöchinger, 1967; Wessely, 2006).

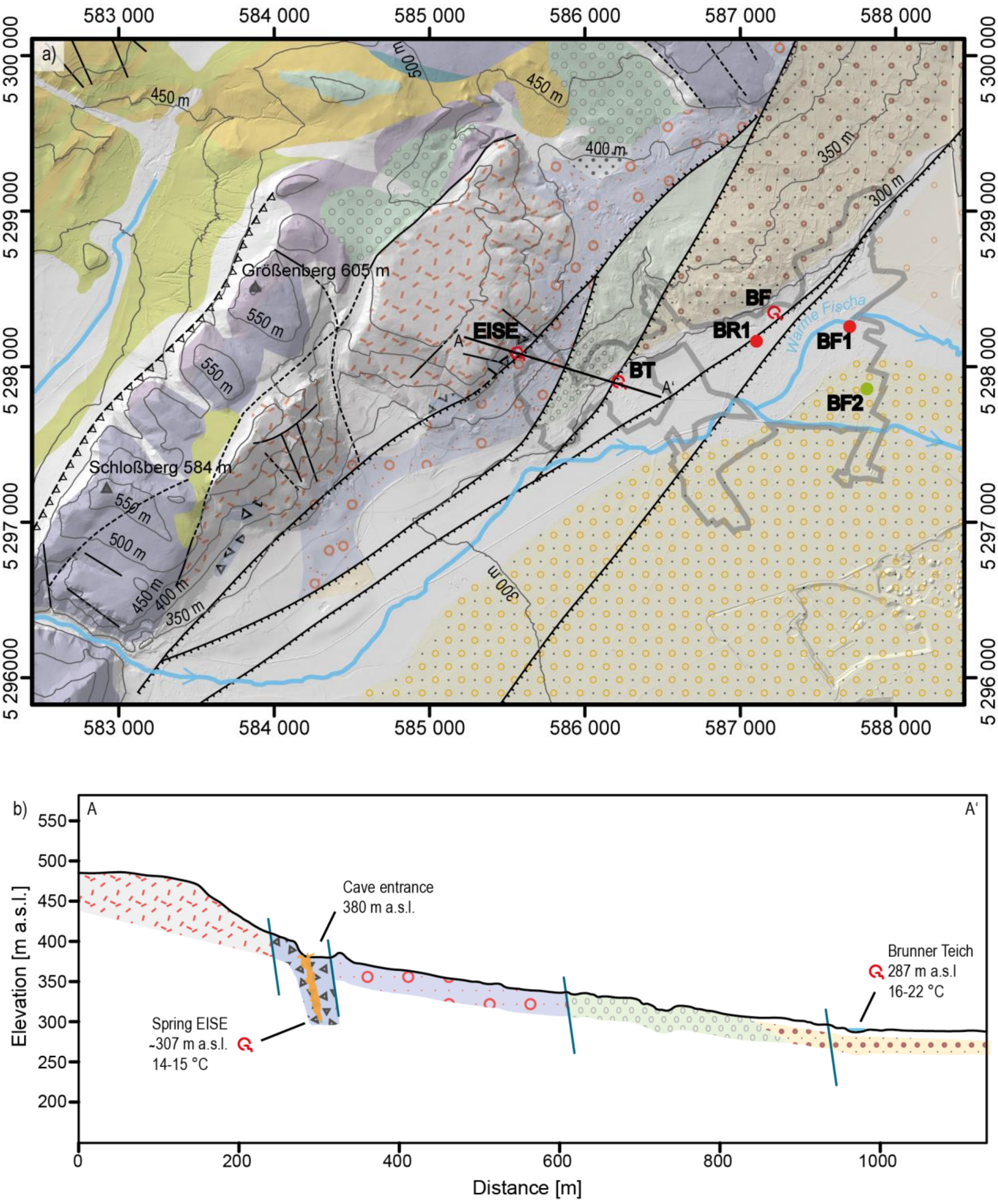

a)
583 000
584 000
585 000
586 000
587 000
588 000
5 300 000
5 299 000
5 298 000
5 297 000
5 296000
450 m
500 m
400 m
350 m
300 m
550 m
Größenberg 605 m
Schloßberg 584 m
EISE
BT
BF
BR1
BF1
BF2
A
A'
Warme Fischa
b)
A
A'
Cave entrance
380 m a.s.l.
Spring EISE
~307 m a.s.l.
14-15 °C
Brunner Teich
287 m a.s.l
16-22 °C
Elevation [m a.s.l.]
Distance [m]

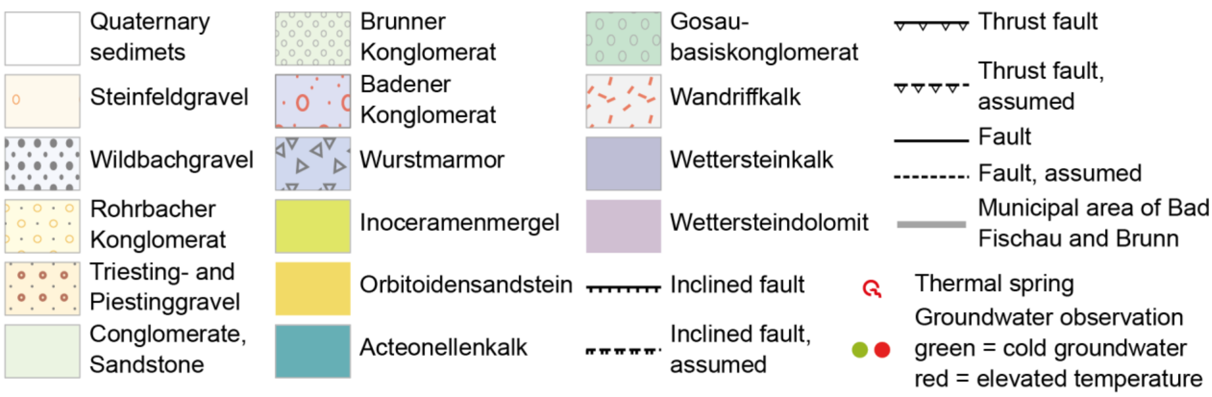

Figure 5: a) Geological Map of the Fischau Hills shown on 1 m – hillshade. Thermal springs: **Eise**nsteinhöhle, **B**ad **F**ischau, **B**runner **T**eich; Groundwater observation points: **B**ad **F**ischau **1**, **B**ad **F**ischau **2** and Bad Fischau **Br**unnen.

b) Cross section through the western margin of the VB cutting EISE and the Brunner Teich in Brunn an der Schneebergbahn. (after Brix, F. and Plöchinger, B., 1982; Plöchinger, B., 1964; topographic data: courtesy Government of Lower Austria); No vertical exaggeration.

2.2.2. Regional tectonic setting

Several major faults run through the area. The left-lateral Salzach-Ennstal-Mariazell-Puchberg (SEMP) fault system extends for about 300 km through greater parts of the Eastern Alps in W-E direction and terminates in the southern VB (Figure 6). With its origin in the central Eastern Alps, the left lateral Mur-Mürztal-Fault System (MM) enters the VB in the south and extends in SE-NW direction through the VB and Moravia into the outer Carpathians. (Hinsch and Decker, 2003). Both, the SEMP and the MM developed during the lateral extrusion of the Eastern Alps in the Miocene, resulting in the opening of the VB along the Vienna Basin Transform Fault, a fault segment of the MM (Royden 1985; Decker, 2005; Baroň et al., 2016).

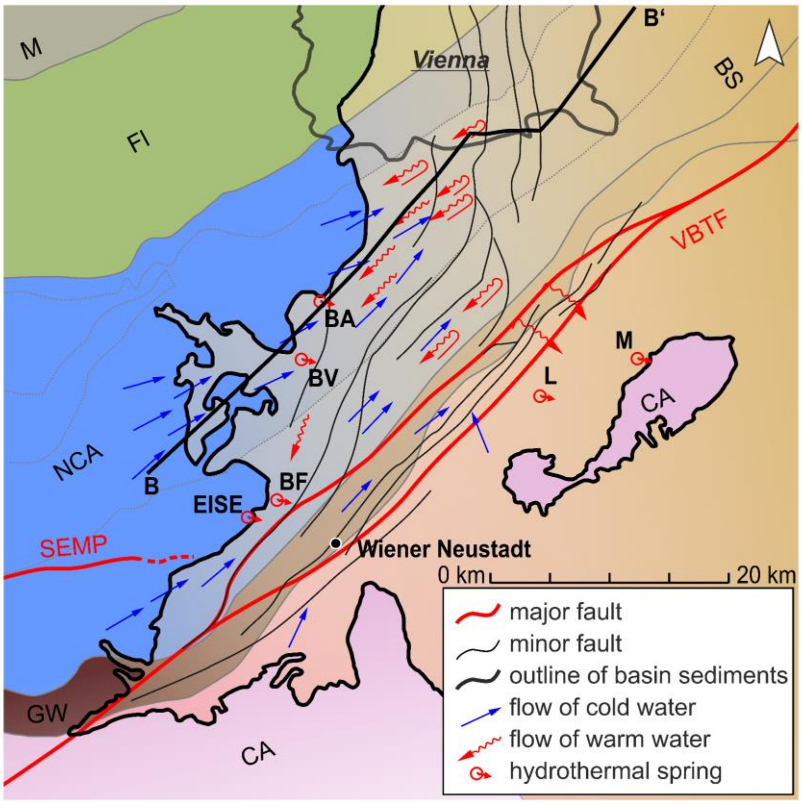

Figure 6: Tectonic map of the southern Vienna Basin and adjacent regions (after Decker et al., 2005 and Wessely, 1983)

Tectonic units: **B**asin **S**ediments; **M**olasse; **Fl**ysch Zone; **N**orthern **C**alcareous **A**lps; **G**rau**w**acken zone, **C**entral **A**lpine;

Thermal springs: **Ba**den, **B**ad **V**öslau, **B**ad **F**ischau, **Eise**n-steinhöhle, **L**eithaprodersdorf, **M**annersdorf

For section B-B' see Figure 8

The western margin of the VB is marked by the Vienna Basin Marginal Fault (VBMF) and several other normal faults are known from the Alpine basement of the VB as well as in the Neogene sediments (Decker et al., 2005; Wessely, 1983).

Recent tectonic activity on these faults becomes apparent as seismic activity throughout the region (Figure 7). Most of the stress is released along the VBTF as earthquakes in the southern part of the VB with a maximum of hypocentres at around 7 km depth (Hinsch and Decker, 2003; Reinecker and Lenhardt, 1999). Hinsch and Decker (2003) calculate a slip rate of up to 0.5 mm/a along some segments of the MM and VBTF making the Southern VB the region with the highest seismic activity in Austria.

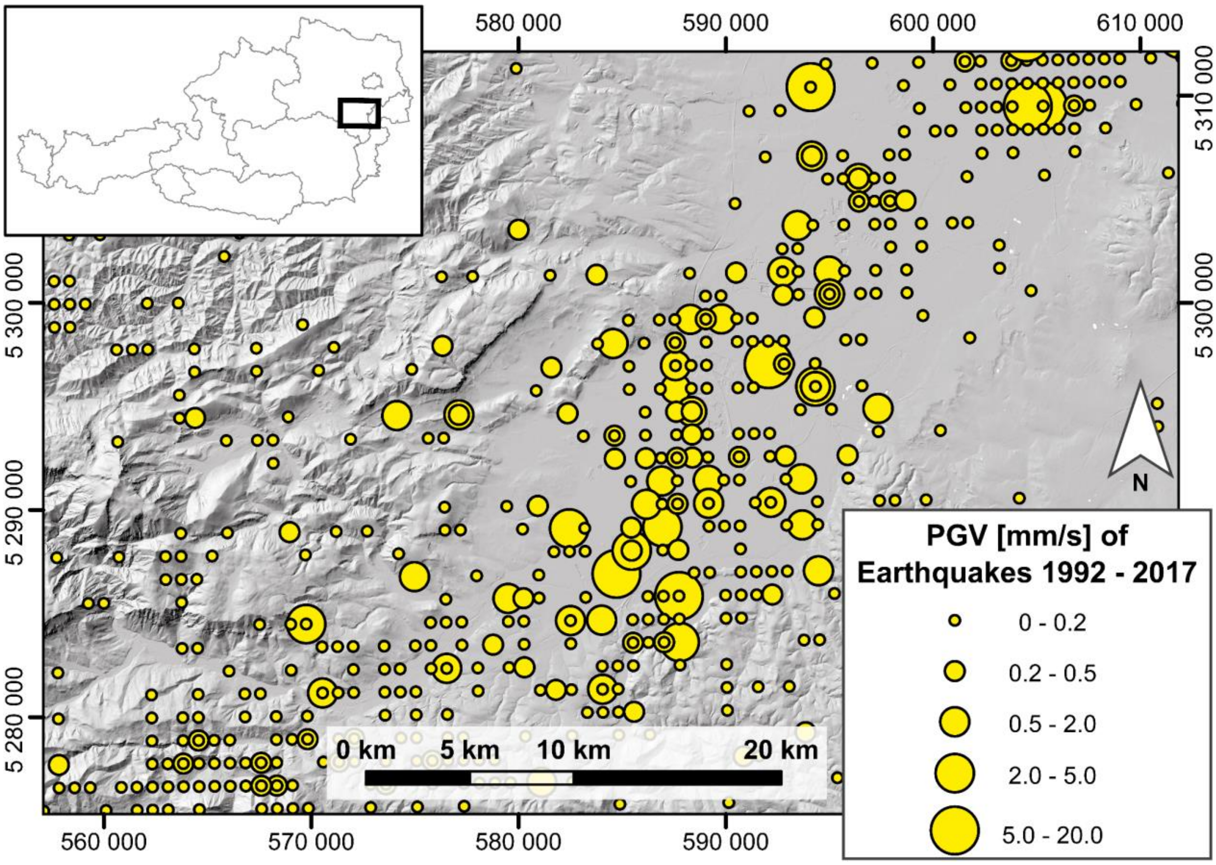

Figure 7: Hillshade of the southern VB (map data: Government of Austria) with calculated peak ground velocities (PGV) of earthquakes at EISE from 1992-2017 (AEC, 2017); Coordinates: UTM 33N.

2.3. Hydrogeology

The VB has been studied extensively during exploration for hydrocarbons and as consequence comprehensive data on hydrogeological processes exist for greater parts. The transition from NCA with its karstified limestones and dolomites to the VB with its filling of mainly clastic sediments substantially influences hydrogeological processes. Borehole data from the fault zone along the western basin margin showed temperature anomalies with warm, highly mineralized groundwater overlying cold water in deeper aquifers (Wessely, 1983).

To explain the temperature anomalies as well as the occurrence of numerous hydrothermal springs along western margin of the VB, a model of groundwater flow was proposed by Wessely (1983). According to that, precipitation infiltrates in the NCA and migrates along fractures and faults in the Alpine Units towards deeper parts of the VB. At depths of up to 6 km the groundwater heats up and rises along faults towards the surface. Fractures and impermeable Neogene sediments channel the thermal groundwater back towards the margin of the VB where the water often mixes with colder groundwater and discharges at several thermal springs (Figure 8).

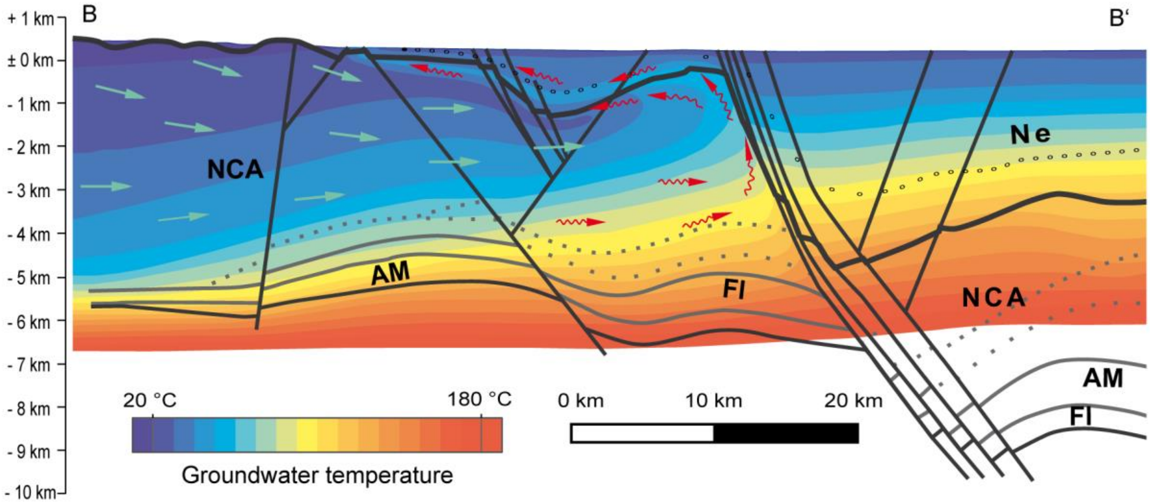

Figure 8: Model of hydrothermal circulation systems along the western margin of the Vienna Basin (after Wessely, 1983). B and B’ refer to Figure 6. Tectonic units: **Ne**ogene sediments, **N**orthern **C**alcareous **A**lps, **Fl**ysch, **A**utochthonous **M**esozoic. Vertical exaggeration: 3 times.

According to Fenzl (1977), who investigated the hydrogeology of Hohe Wand and Fischau Hills, groundwater within the Triassic units of the Hohe Wand Nappe follows fractures and karst systems in NW-SE directions that result from Neogene tectonics.

From hydrochemical and Tritium analysis Fenzl (1977) concluded that precipitation infiltrates in the Hohe Wand area, passes the Neue Welt Basin underground within the limestones of the Hohe Wand Nappe and discharges at springs and rivers east of the Fischau Hills near the margin of the VB.

For the hydrothermal spring in Bad Fischau, (1.6 km east of EISE), Pavuza et al. (1985) suggested a model similar to that of Wessely (1983) but on a smaller scale. Groundwater flows eastward through the karstified rocks of the Fischau Hills towards the VB. Sediments in the VB are less permeable and force the groundwater to flow upwards along the marginal faults. On the surface, it emerges as thermally influenced water.

Elster et al. (2016) suggested this model for all local thermal and subthermal springs (several springs at Spa Bad Fischau, subthermal pond in Brunn and others) and contribute values from hydrochemical and isotope analysis. With around 500 mg/l total dissolved solids the mineralisation in thermal waters near Bad Fischau was found to be relatively low compared to other thermal waters in the VB. δ^{18}O-values of -8.82 to -10.81 ‰ and Deuterium-values of -

64.8 to -76.9 ‰ correspond to recent water in the catchment but a fraction of older groundwater could not be excluded.

2.4. Eisensteinhöhle

2.4.1. General description

EISE was discovered in 1855, during quarrying the Wurstmarmor, the host rock of the cave. Shortly after, most parts of the cave were explored and in 1919 the hydrothermal spring in the deepest part of the cave was discovered (Winkler, 1992).

The cave extends over 87 m in altitude with two entrances at 380 m a.s.l. (located at UTM 33N 585 571 / 5 298 094). The lowest measured point is at -73 m and the highest at +14 m. The maximum horizontal extend is about 150 m in SW-NE direction, the total length is 2.3 km (Hartmann and Hartmann, 2000).

Big boulders and collapsed ceilings dominate the cave morphology in most parts and form a confuse network of galleries (Figure 9, Baroň et al., 2016). However, as characteristic morphologic features like condensation corrosion ceiling half tubes and extremely weathered rock surfaces can be found in some parts, hypogene speleogenesis played a role and at least overprinted the morphology (Spötl et al., 2017).

The cave climate is coined by the hydrothermal activity in the lower parts, leading to temperatures constantly around 13 °C with the highest temperatures near the lukewarm spring. The air in the cave shows elevated CO_2 concentrations of up to 2 % (Plan et al., 2006; Plan and Spötl, 2016;).

EISE is developed in Miocene sediments. The main outcropping unit inside the cave is the Wurstmarmor (Figure 10) and probably towards the upper parts of the cave, the Badener Conglomerate but strongly weathered rock surfaces, the heterogeneity of the Wurstmarmor itself and clay and speleothems (i.e. coralloids, popcorn, frostwork) covering the walls make it hard to define bedding planes or layer boundaries. Cracks permeate the host rock in multiple orientations. They can be closed fissures or as wide as 25 cm and are open, filled with idiomorphic calcite crystals or partially filled with idiomorphic calcite and/or laminated, sandy to loamy sediments. Wessely (2007) describes similar calcite covered cracks in Miocene conglomerates and Triassic carbonates in the borehole “Vöslauer 7” and identifies them as pathways for thermal water.

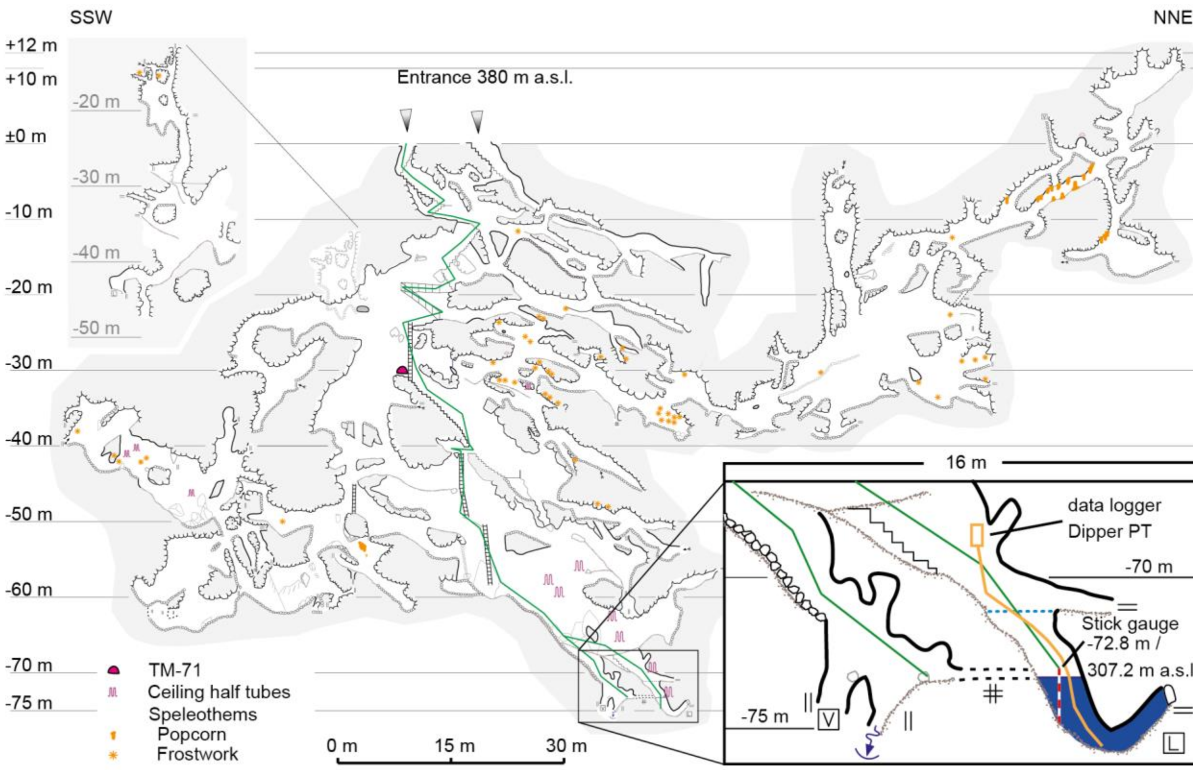

Figure 9: N-S profile of EISE with detail of the lowest parts Lehmbad (left chamber) and Spring (right chamber). Green lines show survey shots from the entrance at 380 m a.s.l. to the reference point at the upper end of the stick gauge at 72.8 m below the entrance. The highest observed water level is marked with a blue dashed line, the overflow from the spring to the Lehmbad is marked by two black dashed lines. (after Nagl and Plan, 2018)

2.4.2. Hydrothermal spring and water level fluctuation

In the deepest part, the cave splits up into two galleries. While the Lehmbad, the lowest lying part of the cave is usually dry, the spring in the neighbouring gallery is almost constantly filled with water (Figure 10). The only few meters thick wall that separates the galleries is fractured and a small crack serves as an overflow in case the water rises high enough. In a few cases when this has happened, the discharge was measured in the Lehmbad. In the Lehmbad the water finally disappears in a narrow fissure.

The water temperature fluctuates around 14.5 °C.

Figure 10: Left: Rock sample of the host rock from EISE. Photograph shows about 15x25 cm; right: Thermal spring with stick gauge and data logger.

3. Materials and Methods

3.1. Time Series Data

This study is based on time series datasets of different parameters including water level and temperature of the hydrothermal spring as well as parameters expectedly influencing the water level of the spring like precipitation and seismic activity.

3.1.1. Water level and temperature data

Gerhard Winkler provided manual measurements of the water level from 1992 onwards. For these measurements, a stick gauge of 2 m length with 10 cm intervals was installed and measurements were taken each time the cave was visited. In rare occasions of overflow, the discharge was measured as the amount of water that reached the neighbouring gallery, but as the water probably drained through other smaller cracks as well, these were only approximations.

The position of the upper end of the stick gauge was referenced at -72.8 m, relative to the cave entrance (380 m a.s.l.) during a cave survey with a vertical accuracy in the range of 10 cm. The accuracy of the stick gauge measurements was tested after the automated data logger was installed in October 2015. These measurements were proven accurate down to ±1 cm.

For automated measurements, a Dipper-PT data logger by SEBA-Hydrometrie with accuracies of ±2.5 mm for water level and ±0.1 °C for temperature and resolutions of was installed (Figure 9). The resolution of these measurements is 0.01 mm and 0.001 °C respectively. Barometric effects on water level measurements are compensated by the logger. The sampling interval was set to 15 minutes.

3.1.2. Seismic data

Seismic data was provided by ZAMG (Zentralanstalt für Meteorologie und Geophysik) as Austrian Earthquake Catalogue (AEC 2017) including all recorded earthquakes from 1992 onwards. The catalogue includes date and time, epicentre location, depth, magnitude and epicentral intensity of the earthquakes. The spatial resolution of the calculated epicentre is 0.01 °, which is roughly 1 km.

3.1.3. Hydrological data

Hydrologic datasets for four meteorological stations and three groundwater heads closest to the cave were provided by the Hydrological Service of Lower Austria (see Table 1 and Figure 4

Precipitation at the stations Miesenbach, Stollhof - Hohe Wand, Saubersdorf and Unterhöflein was recorded as daily total. Distances of the stations to the cave range between 4.8 km for Stollhof and 12.2 km for Miesenbach.

Data on groundwater level at wells 313973 Bad Fischau Br. (BR1), 322560 Bad Fischau BI238 (BF1) and 326900 Bad Fischau BI293 (BF2) was recorded irregularly with some gaps in the datasets. Records of groundwater temperatures at the thermally influenced observation wells had too many gaps for a meaningful analysis.

The nearest well is BR1, 1.6 km, the farthest is BF1, 2.3 km. All wells are located east of the cave in aquifers of the VB.

Table 1: Overview of observation stations. Thermally influenced groundwater observation wells are marked with an asterisk (*). Annual mean temperatures refer to air temperature at meteorological stations and to groundwater temperature for observation wells.

Measured parameter	Name	Coordinate UTM 33N E	N	Distance to EISE [km]	Altitude [m a.s.l.]	Annual mean [mm/a] or [m a.s.l.]	Annual mean temperature [°C]
Precipitation	Stollhof-Hohe Wand	580242	5298028	5.3	446	881.9	8.3
	Saubersdorf	583966	5293635	4.7	320	654.5	8.9
	Unterhöflein	577301	5294065	9.2	441	860.1	8.2
	Miesenbach	573474	5298739	12.1	480	933.2	7.6
Groundwater level	Bad Fischau BR1 *	587127	5298184	1.6	286.5	284.1	11.6
	Bad Fischau BF1 *	587813	5297861	2.3	280.53	266.6	13.4
	Bad Fischau BF2	587724	5298260	2.2	280.76	267.8	–

3.2. Pumping Test

To estimate the volume of the spring as well as to determine its discharge a recovery test was performed in EISE on 13/7/2016, starting from an initial water level of 305.82 m a.s.l. Using an immersion pump, the pumping rate was calculated by taking the time it needed to fill a bucket. The spring was emptied completely, and a small water inlet appeared out of the sandy sediment at the bottom. Its discharge was determined using a measuring cup. During the pumping test, the data logger was set to a 2-minutes sample interval.

3.3. Data analysis

Raw data was prepared with Excel and then processed and analysed using MATLAB (after Trauth, 2006; Menke and Menke, 2012). In MATLAB, Time series data was interpolated with a shape-preserving spline to reduce noise but keep track of short-term changes of water level and temperature and resampled with a sampling interval of 1 day for automatically logged data (October 2015 – October 2017) and a sampling interval of 14 days for long-term observations (1992 – October 2015). This was done to reduce the amount of data for further analysis and visualisation and to synchronize data from different sources. For long-term observations this was also done to have an evenly distributed data array. Data from groundwater wells was treated in the same way.

Daily precipitation data was found unsuitable for correlation with sporadically sampled water level data as data between each sampling point would not be considered in the calculations. Therefore, moving sums for different time intervals (14, 30, 90, 365 days) were calculated and resampled in the same sampling interval as water level data from EISE. Correlations (r-values) and corresponding levels of significance (significant $p \leq 0.05$, highly significant ≤ 0.01) were calculated with the MATLAB function 'corrcoef' (Schönwiese, 2006). Periods with higher correlations were identified with the MATLAB function 'movcorr', that applies a correlation over a moving window of data points.

From seismic data, peak ground velocities (PGV) were calculated for the location of EISE using the equation by Weginger et al. (2017) adapted for the Eastern Alps.

The above-mentioned relation between distance and magnitude for earthquake-related hydrogeologic phenomena described in the literature (Montgomery and Manga 2003) was used to decide if earthquakes are relevant for water level changes at EISE.

3.4. Observations of tectonic structures in the field

On several occasions measurements of structural features were taken. These measurements included dip and dip direction of joints, calcite veins and slickensides and where possible, direction and sense of shear. Measurements were visualised with OpenStereo.

4. Results

Due to different methods of data collection, the data availability is unsteady. In the first phase (1992-2015) when data was collected manually sampling rates ranges from of one measurement per year to more than one in two weeks. The average sampling rate was about one sample per month. In the second phase (October 2015 – November 2017) the sampling rate was much higher and therefore, time series data is split into two sections for further analysis.

4.1. Period of manual water level observations (1992 – 2015)

4.1.1. Water level changes

During the first observation period a drying-up as well as several overflow events into the neighbouring gallery were observed.

The record of water level shows fluctuations within a range of 3.9 m with 304.8 m a.s.l. as minimum and 308.7 m as maximum values (Figure 11). Certain stages can be considered as recurring, such as levels around 306 m a.s.l. which were observed on 47 occasions and around 307.10 m with 93 counts. Levels around the average water level of 306.5 m a.s.l. were observed only few times. This leads to a bimodal frequency distribution of observed water levels (Figure 12).

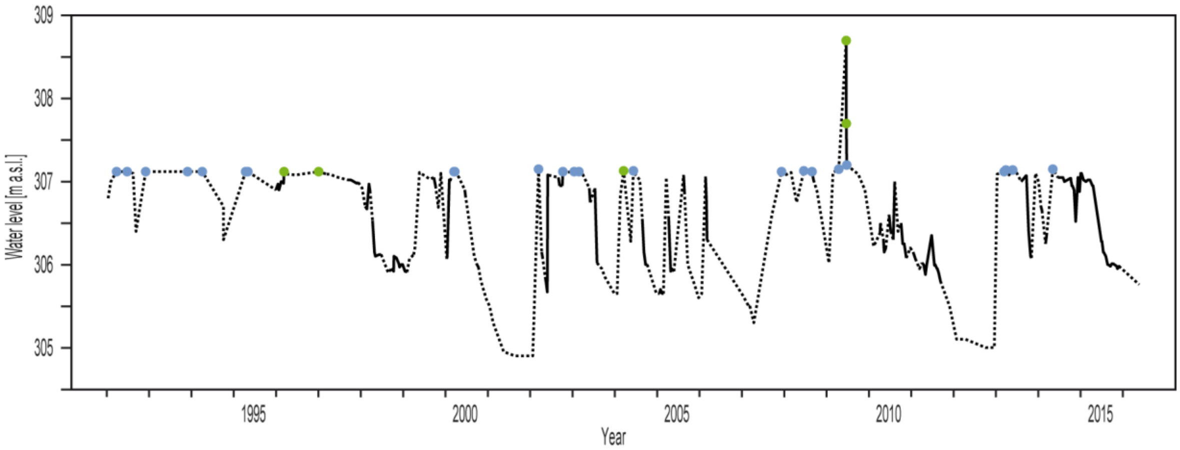

Figure 11: Water level of the spring at EISE recorded by Gerhard Winkler. Blue dots indicate overflow into the Lehmbad, green dots indicate flooding of the Lehmbad, dotted lines indicate a sampling interval of more than 21 days, the full line indicates sampling intervals of 21 days or less

The lowest level was observed over several months in 2001 when only a small amount of water remained in the spring while the highest level was reached on 29/6/2009 after the overflow was not able to take all water and a back flooding of 150 cm above the upper end of the stick gauge occurred (Figure 13). 21 discharge measurements during overflow conditions ranged from

4.2 l/h to 289 l/h. Discharges higher than 240 l/h can lead to flooding of the Lehmbad and prevent discharge measurements. This was observed 5 times

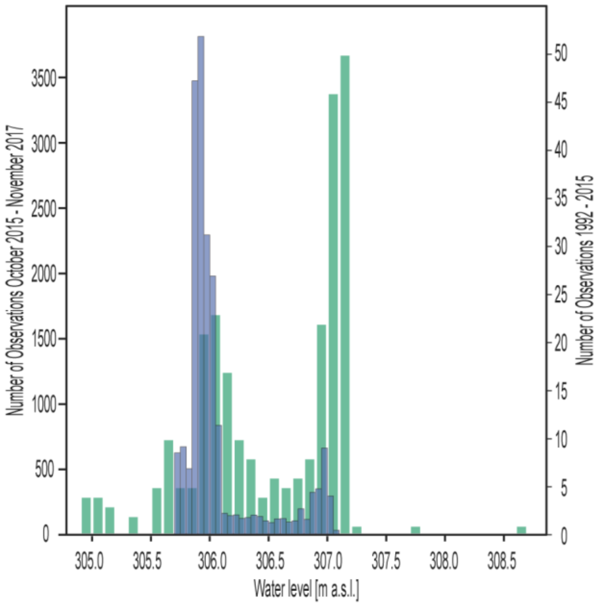

Figure 12: Frequency distribution of hourly observed water levels during automated measurements in blue and sporadic measurements from 1992 until 2016 in green. Values during the pumping test is excluded. The higher number and resolution of automated measurements compared to the sporadically collected data allow smaller class sizes.

Figure 13: Turbid and foamy water during the days of the highest water level in June 2009. Photo: Gerhard Winkler (27/6/2009).

4.1.2. Correlation with precipitation data

The correlation of water level at EISE and 14-day precipitation sums is weak for all stations. By increasing the number of days over which precipitation is integrated (Figure 14), the correlation increases to moderate (see Table 2). The strongest correlation was found for Stollhof ($r = 0.63$; $p \leq 0.01$) followed by Miesenbach ($r = 0.62$; $p \leq 0.01$) for precipitation sums of 365 days. The precipitation at these stations is very similar in distribution ($r = 0.89$; $p \leq 0.01$) and therefore only data from Stollhof was investigated further.

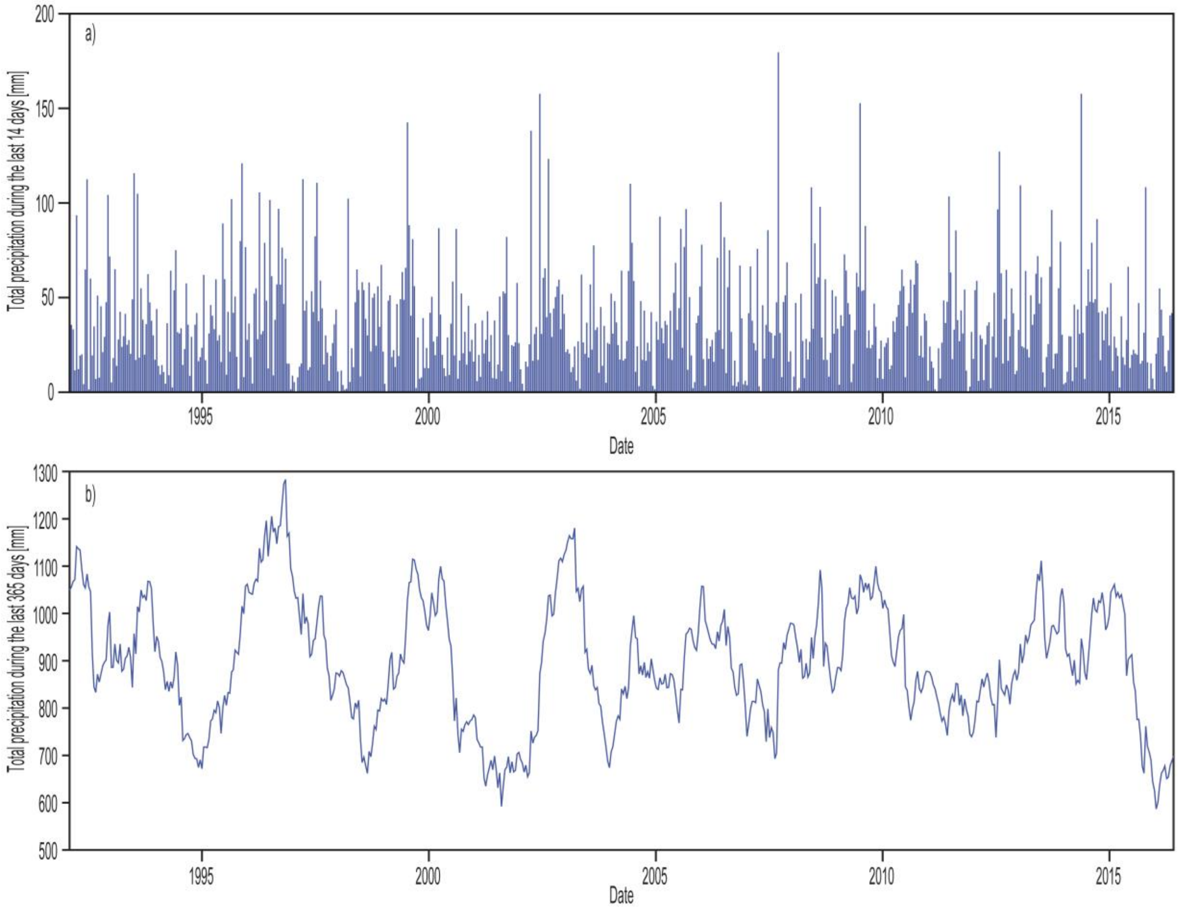

Figure 14: a) 14-day precipitation sum at station Stollhof and. b) 365-day precipitation, both resampled in the same two weeks interval as the water level.

Table 2: Correlation coefficient for water level at EISE and total precipitation over the previous 14, 90 and 365 days for each sampling date.

	14 days	90 days	365 days
Stollhof	0.13	0.30	**0.63**
Miesenbach	0.13	0.27	0.62
Unterhöflein	0.11	0.24	0.44
Saubersdorf	0.11	0.17	0.35

Correlation over a moving window indicates a change of correlation between precipitation and water level at EISE over time. The period from November 1998 until August 2001 (Figure 15) for example shows a strong correlation ($r = 0.90$; $p \leq 0.001$).

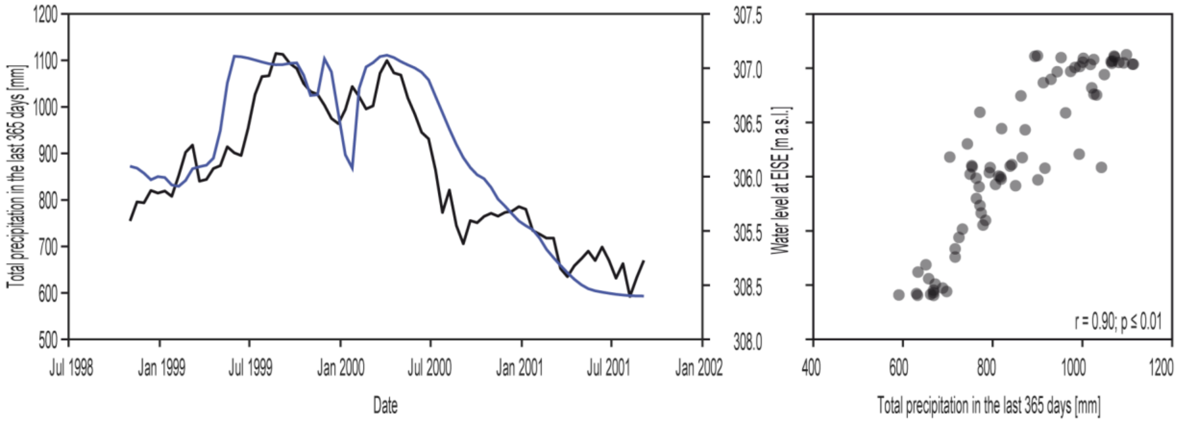

Figure 15: Accumulated precipitation of the previous 365 days for each sampling date (black) and water level at EISE (blue) from winter 1998 until autumn 2001 with the corresponding scatterplot.

The poor correlation of short-term precipitation data and water level is inconsistent with observations during manual measurements, when thunderstorms and extreme rainfall preceding the highest measured water level on 29/6/2009 were noted down. Several days of intense rainfall with 156.3 mm within 10 days and a maximum of 40 mm/d at the nearest Station Stollhof occurred.

4.1.3. Correlation with groundwater in nearby wells

The water level at EISE is about 24 m above the groundwater at well BR1 and about 40 m above groundwater at wells BF1 and BF2 (Figure 16). Although the latter have a higher difference in head and are further away, correlation for these two is stronger than for BR1. BF2 with the strongest correlation was investigated further and a time shift of about 14 weeks giving the best correlation ($r = 0.78$; $p \leq 0.01$) was identified (Figure 17).

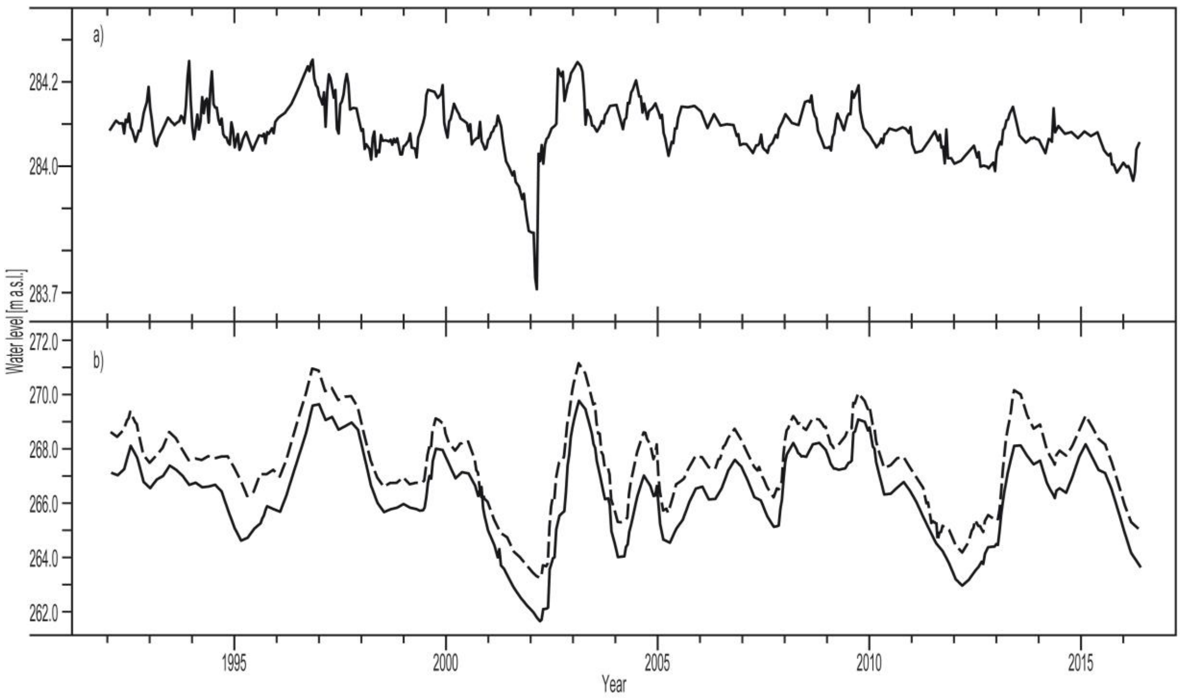

Figure 16: Groundwater levels at nearby wells from 1992 until 2016: a) BR1; b) BF1 (full line) and BF2 (dashed line).

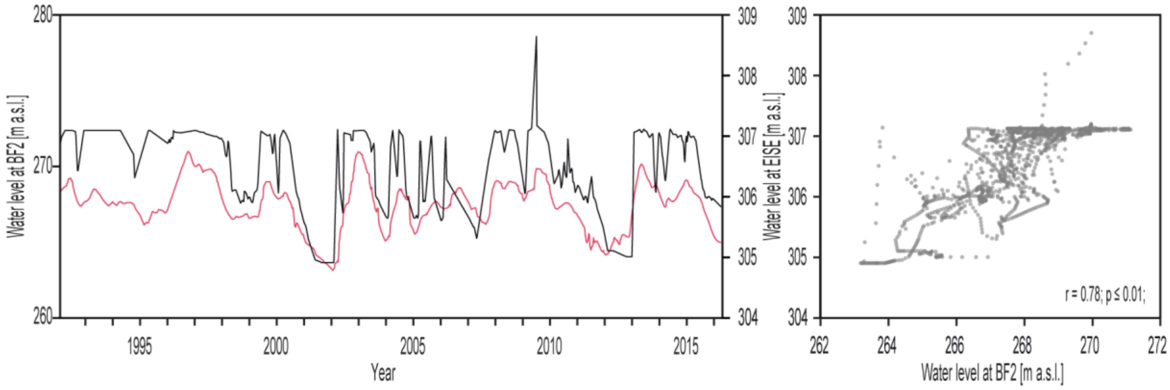

Figure 17: Correlation of water levels at EISE (black) and BF2 (red). The 14-weeks delay of BF2 is removed in this figure for a better visualization of the correlation. R increased from 0.68 to 0.78 compared to correlation without delay.

4.2. Period of automated measurements October 2015 to November 2017

4.2.1. Water level and temperature changes

During automated measurements, the water level seemed to be more or less steady, apart from five events (Figure 18) of water level increase. No natural drying out was observed but during the pumping test the spring was emptied completely. The part of the data set, from the start of the pumping test until the initial water temperature was reached again, was considered to be influenced and is analysed separately. The natural water level fluctuations within 40 cm around 306 m a.s.l. with events of sudden increase peaking up to 307.09 m a.s.l. It also showed a different frequency distribution than during manual measurements (Figure 12; Figure 19). The peaks of the, again bimodal, distribution are located around the same values, but 306 m a.s.l. is the more prominent one. During the high discharge events, the water level stagnates for a short time just below the visible overflow.

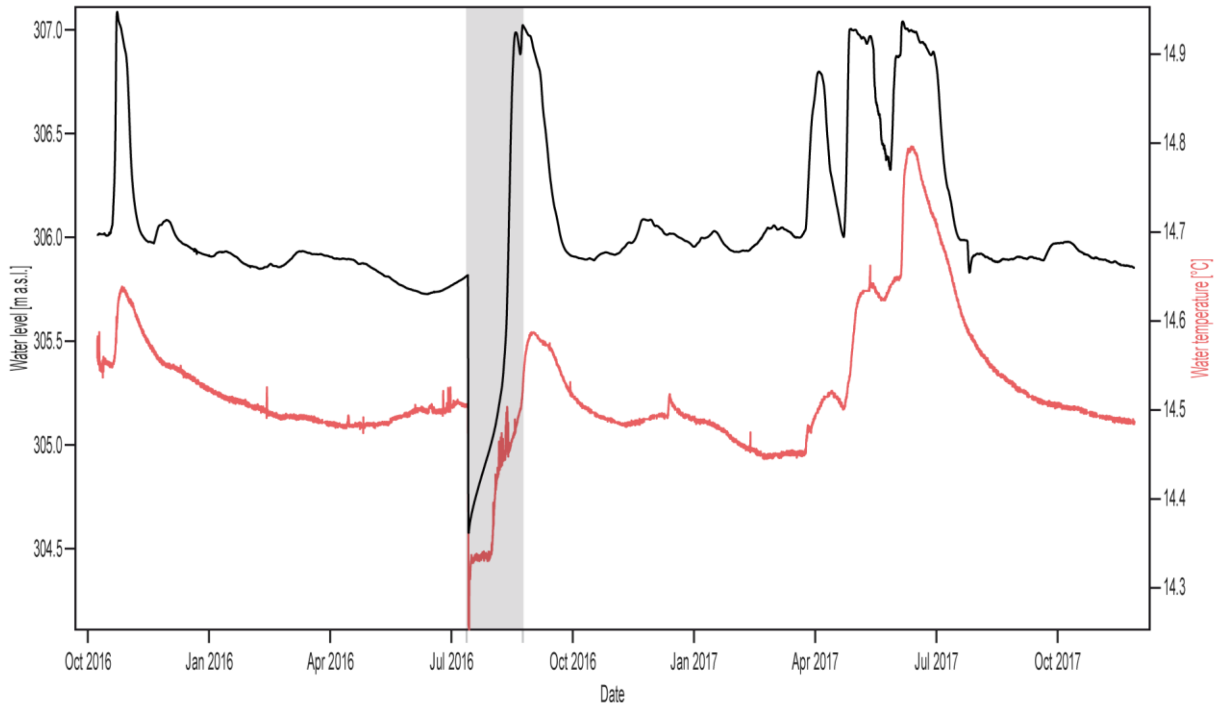

Figure 18: Observed water level (black) and temperature (red) at EISE from October 2015 until November 2017. The data presumably influenced by the pumping test (13/7/2016-22/8/2016) is marked by the grey area.

The temperature ranged between 14.4 °C and 14.8 °C. During high discharge events, temperature increases always followed the water level with a delay of 4 to 15 days and cooling took longer than for the water level reaching the initial stage. From March 2017 to August 2017 three of these high discharge events were recorded. While the water level drops significantly between each of the events, the temperature is reduced slightly before it rises again with the next water level increase. In this way, the temperature rises for in total 0.35 °C in three steps (Figure 20)

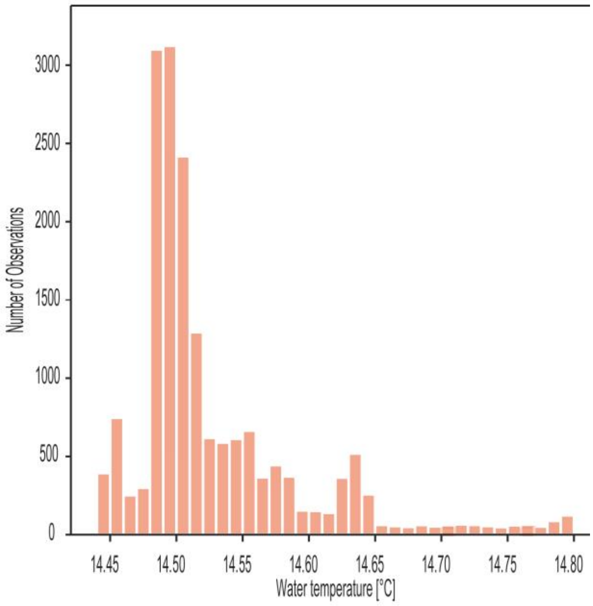

Figure 19: Frequency distribution of observed hourly water temperatures from Oct. 2015 until Nov. 2017. Data of the pumping test is excluded.

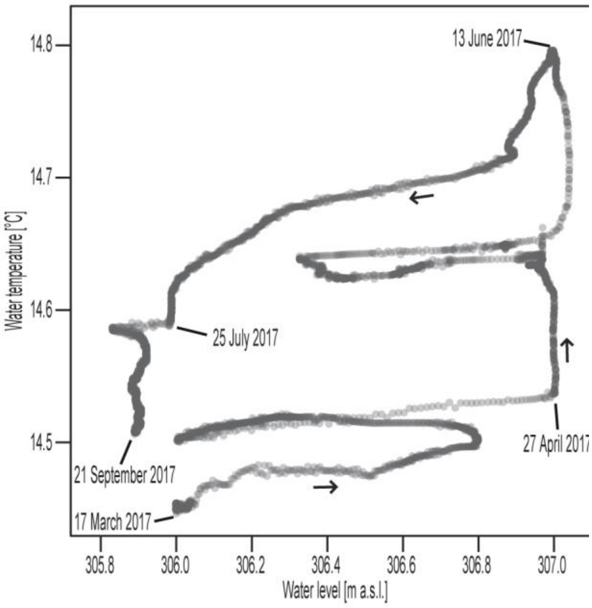

Figure 20: Scatterplot of hourly measured water levels and corresponding temperatures for the period of March 2017 until August 2017. The delay of temperature changes is well visible.

4.2.2. Pumping test

On 12/6/2016 a pumping test was performed inside the cave. The determined pumping rate was about 1.7 l/s (with a standard deviation of 5.9 %) which emptied the spring in 28 minutes leading to a pumped volume of about 2.8 m^3 (± 0.16 m^3).

The lowest measured water level of 304.58 m a.s.l. was reached during the pumping test when the water level dropped slightly below the lowest measurable head. When the spring was emptied completely, a small outlet in the sandy bottom appeared to be the water source.

The amount of water that was discharged in the following three hours was measured using a measuring cup giving the discharge rate of 5.7 l/h. This rate is rather low compared to discharges that were measured during overflow events. Assuming above mentioned volume and a constant discharge, the spring would have been filled to the same level after ca. 20 days. The actual time until the initial water level was reached was 31 days.

During the pumping test, the temperature fell from 14.51 °C to 14.17 °C, the lowest recorded temperature.

4.2.3. Correlation of the spring level with precipitation

No clear correlation between the automatically recorded water level at EISE and precipitation was found. However, all major and some minor water level increases followed days with precipitation of 15 mm or more. In turn, not all days with precipitation of 15 mm or more were followed by distinct water level changes (Figure 21)

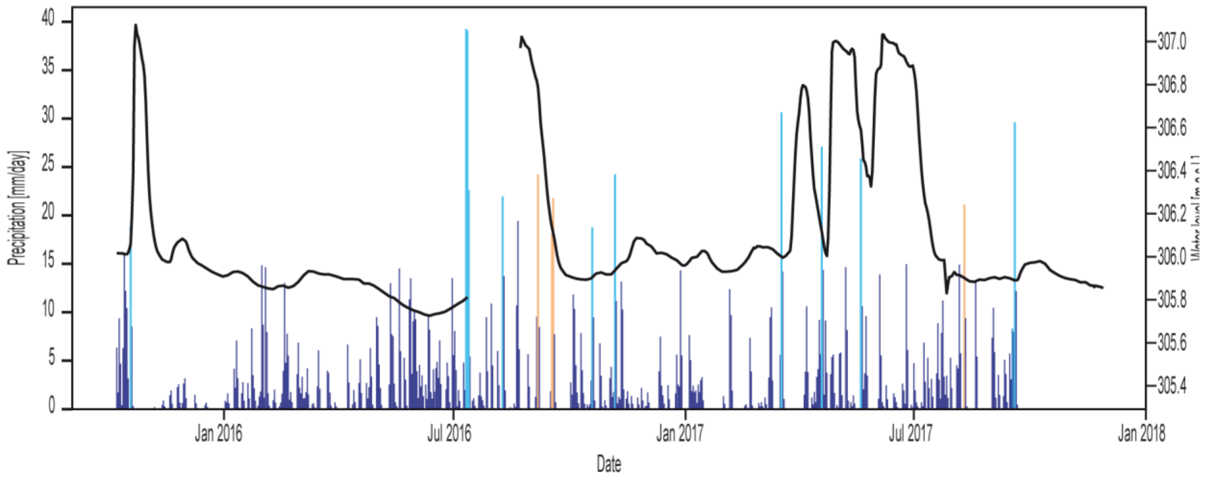

Figure 21: Daily precipitation at station Stollhof and water level at EISE. Light blue bars indicate rain events with more than 15 mm in 24 hours, that were followed by a water level increase. Orange bars indicate such events that were not followed by an increase. Note that there are also distinct peaks with no preceding rain events exist.

4.2.4. Correlation with groundwater in the Vienna Basin

For groundwater wells, no correlation was found in the short-term observations.

4.2.5. Comparison of water level and temperature changes with seismic data

Comparing the water level with seismic data, only few events causing considerable PGV at EISE are relevant. Only one remarkable water level change at the end of July 2017, which cannot be related to precipitation stands out (Figure 22). At an initially constant condition, the water dropped 20 cm in one day before it recovered simultaneously to several earthquakes of magnitude ≤ 2.4 in a radius of 2 km (Figure 23).

The epicentres of most of these earthquakes were located in Bad Fischau, but the strongest one with a magnitude of 2.4 was located further west only 1 km from the cave at a depth of 5.1 km.

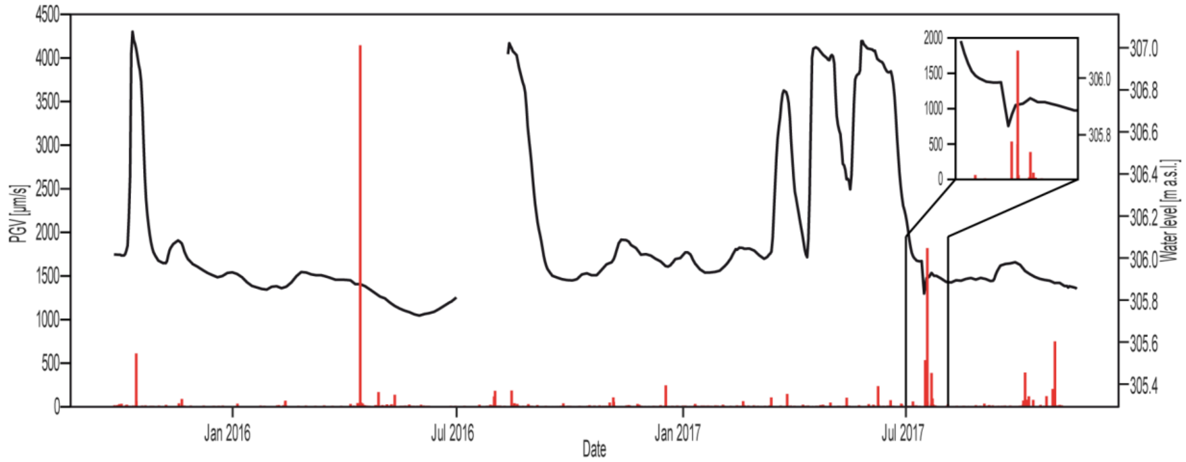

Figure 22: Peak ground velocities calculated for the location of EISE and for reference the recorded water level. Only few earthquakes cause noteworthy ground motion at EISE.

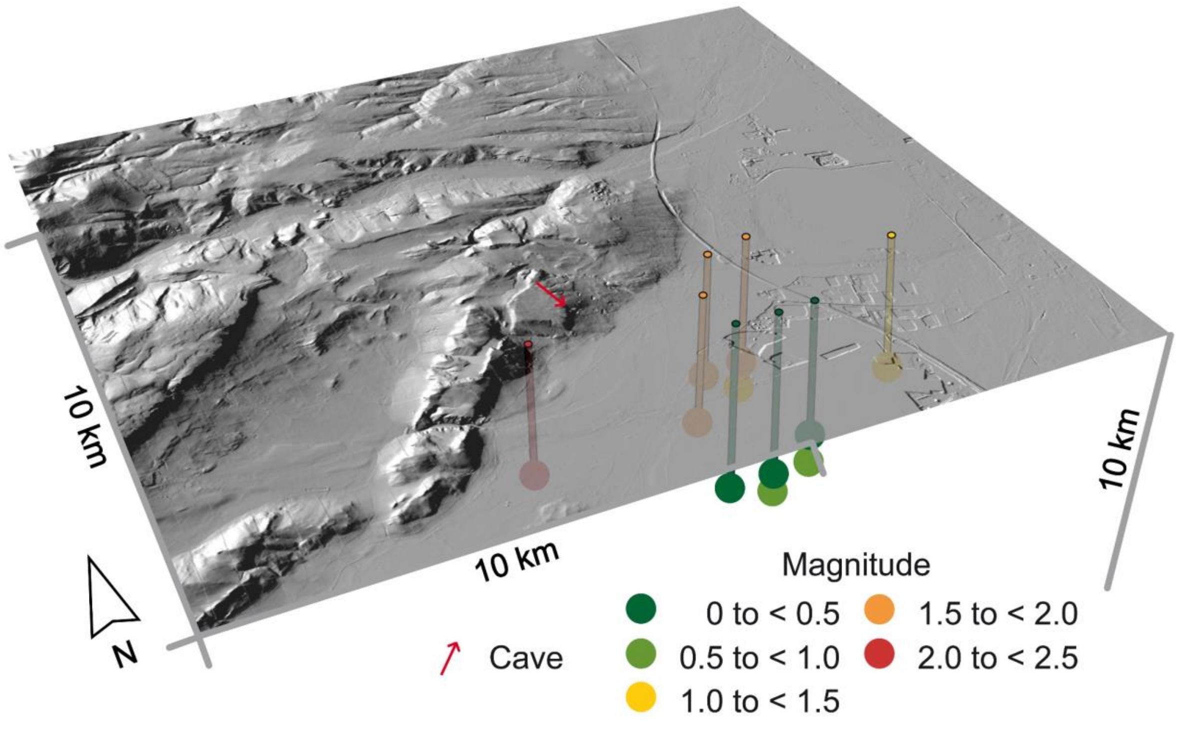

Figure 23: Hillshade (topographic data: courtesy of Government of Lower Austria) with hypocentres of earthquakes following the sudden water level decrease at the end of July and beginning of August 2017.

4.3. Measurements structural features

17 structural features were measured inside the cave, thereof 11 calcite veins, 3 joints and 3 slickensides with lineation. On the slickensides the direction, but not the sense of shear could be identified Figure 24.

Calcite veins (Figure 25)share the orientation of strike in NNE-SSW direction with a dip between 42 and 86 ° towards NW with one vein inconsistently dipping towards SE. Slickensides are all oriented NW-SE dipping around 85 ° with a lineation indicating almost vertical direction of displacement. The measured joints also show a NE-SW strike but dip towards SE-directions.

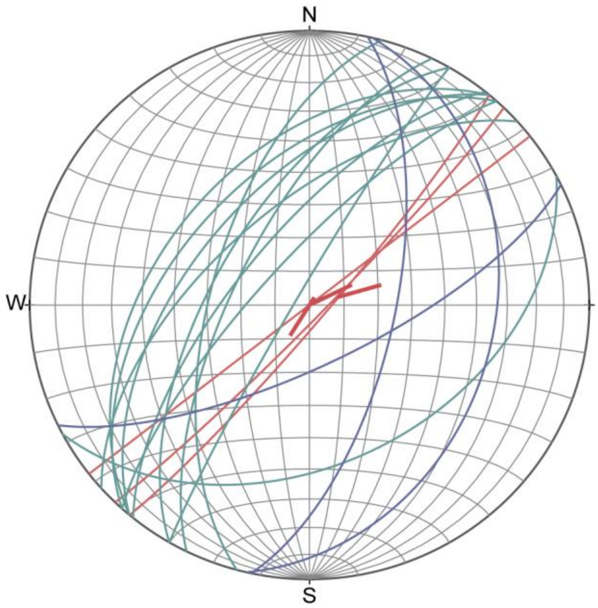

Figure 24: Stereographic projection of planes measured inside the cave. red: slickensides; blue: joints; green: calcite veins.

Figure 25: Calcite vein partially filled with clay. Photo: L. Plan.

5. Interpretation and Discussion

5.1. Water level and temperature records

In general, the quality of both collected datasets is suitable for time series analysis and manual measurements, taken during the automated logging, showed a precision of ± 1cm. However, the scarcity of data points during some intervals of manual measurements complicate the correlation with other datasets and even make it useless for correlations with seismic data that consist of single points in time. Data interpolation often results in repetitive values or linear trends (e.g. periods 1992-1994, 2006-2008). This is also reflected in the correlation of the interpolated data with short-interval precipitation data (Table 2).

Furthermore, manual measurements show a bias towards higher water levels than during the period of automated measurements (U-test rejected the hypothesis of equal medians). This could either mean, that a sustained change of the water level occurred or that the cave was visited more often during higher water levels. No influence of seasonal variations of the frequency of measurements was found. Comparing the two records, it becomes apparent that peaks of only few weeks in the record of automated measurements are probably represented as plateaus of several months during manual observations. Especially when high water levels are interpolated, the bias introduced by the measurement is amplified by interpolation.

The high-water levels show plateaus, indicating that the pool drains through unknown outlets. From this follows that the discharge measurements made during overflow conditions underestimate the actual discharge to an unknown extent which confirms this assumption by Winkler (1992).

Water level and temperature are coupled with a delay for the temperature of 4 to 15 days. This time shift is interpreted as the time it takes for the warm water to flow through a crack or conduit, initially filled with colder water and to warm up the surrounding rock. The fact that not all water level changes are followed by increasing temperature hint towards multiple water sources that feed the spring.

5.2. Pumping test

The pumping test helped to clearly identify a diffuse outlet in the sandy bottom of the spring as the water inflow. However, it gave no exact insight into aquifer properties but rather constraints to integrate this particular spring into the hydrogeological setting.

The fact that the neighbouring Lehmbad is at the same elevation as the spring indicates that the spring is fed by a small, vadose conduit and not directly connected with a bigger body of karst water of the Fischau Hills. The actual water level of the spring is determined by the balance of discharge and outflow through several small, undetected fissures.

5.3. Correlations with other datasets

The correlation with meteorological stations reveal a major influence of precipitation on water level changes at EISE. In particular, the accumulated precipitation at the stations west of EISE show a robust correlation.

Combining observations of both, long-term and short-term records lead to a model with a reservoir that, when filled to a certain level, responds to single precipitation events like it was observed during automated measurements. Inside this reservoir, mixing of waters of direct meteorological and deep seated hydrothermal origin is likely.

Hydrogeolocigal models by Wessely (1983) and Pavuza et al. (1985) describe a north-east to east directed groundwater flow in the Fischau Hills. This is in agreement with the 8 weeks delay of groundwater signals at BF1 relative to EISE and indicates that both observation points are in the same aquifer or that groundwater at these points is influenced by the same factors.

The comparison with seismic data shows that there are earthquakes relevant for inducing hydrogeological effect at EISE, but also that they do not occur very often. However, the rare and irregular occurrence of earthquakes, that cause enough strain or ground shaking at EISE to induce hydrogeological effects made it impossible to verify the relation and to analyse the processes behind so far.

5.4. Interpretation of structural measurements

The NE-SW trend of all measured structural features is consistent with orientations of the fault zone on the western margin of the VB. The appearance and the orientation of calcite veins are similar to those encountered in the borehole ‘Vöslauer 7’ described by Wessely (2007) and their occurrence suggest a former circulation of hydrothermal fluids through higher parts of EISE and its hostrock.

6. Conclusion

The thermal spring in the lowest part of Eisensteinhöhle shows fluctuations in discharge resulting in water levels between 304.8 and 308.7 m a.s.l. The observed discharges ranged from 4.2 to 289 l/h. The highest water level was observed on 29/6/2009, after a period of intense rainfall with 156.3 mm in 10 days. A complete drying-up happened over several months in 2001.

The water level of the spring is determined by the equilibrium of the discharge and the outflow through cracks and fissures. The most prominent levels in the frequency distribution of water levels indicate the position of cracks or more permeable rock. Certain recurring water levels like 306 and 307.1 m a.s.l. indicate the position of these partially unseen outlets.

The water temperature ranged between 14.4 and 14.8 °C and is positively correlated with the spring discharge. During high discharge events, the increase of water temperature followed the increase of water level with a delay of 4 to 15 days.

A pumping test revealed the actual inlet of the spring and helped to interpret water level as well as discharge data.

The analysis of two different datasets showed that the spring discharge in the deepest part of Eisensteinhöhle is controlled by several factors.

On a long-term base, the annual average of precipitation plays a dominant role. However, short-term observations showed, that water level fluctuations are more complex and only single rainfall events that were responsible for an increase in water level could be identified. However, the magnitude of influence of individual factors stays uncertain and probably changes over time.

In the greater picture, it was also shown that the aquifer feeding the hydrothermal spring, is in contact with the aquifer in the nearby wells in the Vienna Basin or is at least influenced by the same factors. As water level changes are more abrupt, the spring is probably closer to the catchment and signals from precipitation events get attenuated.

Furthermore, it was shown, that even sporadically collected hydrological data can be helpful for this kind of analysis even though temporal resolution is not very high. By very simple means, a quite long and more or less continuous water level record was created, enabling time series analysis.

Concerning the correlation with seismic data first events could be identified, but in order to have a higher number of earthquakes that cause ground motion at Eisensteinhöhle and its surroundings a much longer observation would be necessary.

7. References

AEC, 2017. Austrian Earthquake Catalogue – Computer file. Seismological Service of Austria, Department of Geophysics, Zentralanstalt für Meteorologie und Geodynamik (ZAMG).

Baroň, I., Plan, L., Grasemann, B., Mitrovic, I., Lenhardt, W., Hausmann, H. and Stemberk, J., 2016. Can deep seated gravitational slope deformations be activated by regional tectonic strain: First insights from displacement measurements in caves from the Eastern Alps. Geomorphology, 259, 81–89. https://doi.org/10.1016/j.geomorph.2016.02.007

Brix, F. and Plöchinger, B., 1982. Wiener Neustadt 1:50000. In: Geologische Bundesanstalt. Geologische Karte der Republik Österreich 1:50000, 76, Verlag der Geologischen Bundesanstalt, Vienna.

Brodsky, E.E., 2003. A mechanism for sustained groundwater pressure changes induced by distant earthquakes. Journal of Geophysical Research, 108/B87, 2390. https://doi.org/10.1029/2002JB002321

Cooper, H., Bredehoeft, D. and Robert, R., 1965. The Response of Well-Aquifer Systems to Seismic Waves. Journal of Geophysical Research, 70/16, 3915–3926.

Decker, K., Peresson, H. and Hinsch, R., 2005. Active tectonics and Quaternary basin formation along the Vienna Basin Transform fault. Quaternary Science Reviews, 24, 307–322. https://doi.org/10.1016/j.quascirev.2004.04.012

Elster, D., Goldbrunner, J., Wessely, G., Niederbacher, P., Schubert, G., Berka, R., Philippitsch, R. and Hörhan, T., 2016. Erläuterungen zur geologischen Themenkarte Thermalwässer in Österreich 1:500000. Geolocigal Survey of Austria, Vienna, pp. 296.

Fenzl, N., 1977. Hydrogeologische Studie des Gebietes Hohe Wand und Fischauer Berge. Verhandlungen der Geologischen Bundesanstalt, 2, 121–164.

Grünthal, G., Musson, R., Schwarz, J. and Stucchi, M., 1998. European Macroseismic Scale 1998. Conseil de l'Europe - Cahiers du Centre Européen de Geodynamique et de Seismologie, 15, Centre Europèen de Géodynamique et de Séismologie, Luxembourg, 99 pp.

Hartmann, H. and Hartmann, W., 2000. Die Höhlen Niederösterreichs – Band 5. Die Höhle, Supplement 54.

Hinsch, R. and Decker, K., 2003. Do seismic slip deficits indicate un underestimated earthquake potential along the Vienna Basin transfer fault system? Terra Nova, 15/5, 343–349. https://doi.org/10.1046/j.1365-3121.2003.00504.x

Hock, R., 1948. Thermenwasser aus der Eisensteinhöhle bei Brunn an der Schneebergbahn. Unveröffentlichter Bericht, Wien.

Lai, G., Jiang, C., Han, L., Sheng, S. and Ma, Y., 2016. Co-seismic water level changes in response to multiple large earthquakes at the LGH well in Sichuan, China. Tectonophysics, 679, 211–217. https://doi.org/10.1016/j.tecto.2016.04.047

Larsson, I., 1972. Ground water in granite rocks and tectonic models. Nordic Hydrology, 3, 111–129. https://doi.org/10.2166/nh.1972.0008

Menke, W. and Menke, J., 2012. Environmental data analysis with Matlab. Elsevier, Oxford, pp. 288. https://doi.org/10.1016/C2010-0-69111-5

Michetti, A.M., Esposito, E., Guerrieri, L., Porfido, S., Serva, L., Tatevossian, R., Vittori, E., Audemard, F., Azuma, T., Clague, J., Comerci, V., Gürpinar, A., Mc Calpin, J., Mohammadioun, B., Mörner, N.A., Ota, Y. and Roghozin, E., 2007. Environmental Seismic Intensity Scale ESI 2007. In Memorie descrittive della carta geologica D'Italia. L. Guerrieri & E. Vittori (ed.), Servizio Geologico d'Italia, Dipartimento Difesa del Suolo, APAT, Rome, Italy, 74, 7–54.

Mogi, K., Mochizuki, H. and Kurokawa, Y., 1989. Temperature changes in an artesian spring at Usami in the Izu Peninsula (Japan) and their relation to earthquakes. Tectonophysics, 159, 95–108. https://doi.org/10.1016/0040-1951(89)90172-8

Montgomery, D.R. and Manga, M., 2003. Streamflow and Water Well Earthquakes. Science, 300, 2047–2049. https://doi.org/10.1126/science.1082980

Mühlhofer, F., 1923. Die Eisensteinhöhle nächst Bad Fischau und Brunn am Steinfeld (Niederösterreich). Österreichischer Höhlenführer, 4, Wien.

Muir-Wood, R. and King, G.C.P., 1993. Hydrological signatures of earthquake strain. Journal of Geophysical Research, 98/B12, 22035–22068. https://doi.org/10.1029/93JB02219

Pavuza, R., Prohaska, W. and Traindl, H., 1985. Blatt 76 – Wiener Neustadt. Karstverbreitungs- und Karstgefährdungskarten Österreichs 1:50000. Verband österreischischer Höhlenforscher, Wien, pp. 67.

Pirker, R., 1950. Temperaturbeobachtungen in der Eisensteinhöhle. Protokoll der 5. ordentl. Vollvers. d. Höhlenkomm, beim Bundesministerium f. Land- und Forstwirtschaft in Wien am 23. und 24. 10. 1950 in Peggau, Steiermark, Wien.

Plan, L., Pavuza, R. and Seemann, R., 2006. Der Nasse Schacht bei Mannersdorf im Leithagebirge, NÖ (2911/21) – eine thermal beeinflusste Höhle am Ostrand des Wiener Beckens. Die Höhle, 57/1-4, 30-46.

Plan, L. and Spötl, C., 2016. Hypogene Karsthöhlen. In: C. Spötl, L. Plan, E. Christian (ed.). Höhlen und Karst in Österreich, Oberösterreichisches Landesmuseum, Linz, 49–60.

Plöchinger, B., 1967. Erläuterungen zur Geologischen Karte des Hohe-Wand-Gebietes (Niederösterreich) 1:25.000, Verlag der Geologischen Bundesanstalt, Vienna, pp. 142.

Plöchinger, B., 1964. Geologische Karte des Hohe Wandgebietes (Niederösterreich) 1:25000. Verlag der Geologischen Bundesanstalt, Vienna.

Reinecker, J. and Lenhardt, W.A., 1999. Present-day stress field and deformation in eastern Austria. International Journal of Earth Sciences, 88, 532–550. https://doi.org/10.1007/s005310050283

Roeloffs, E.A., 1988. Hydrologic precursors to earthquakes: A review. Pure and Applied Geophysics, 126/2–4, 177–209. https://doi.org/10.1007/BF00878996

Roeloffs, E.A., 1996. Poroelastic Techniques in the Study of Earthquake-Related Hydrologic Phenomena. Advances in Geophysics, 37, 135–195. https://doi.org/10.1016/S0065-2687(08)60270-8

Rojstaczer, S., Wolft, S. and Michel, R., 1995. Permeability enhancement in the shallow crust as a cause of earthquake-induced hydrological changes. Nature, 237–239. https://doi.org/10.1038/373237a0

Royden, L.H., 1985. The Vienna Basin – A Thin-Skinned Pull-Apart Basin. In: Biddle, K.T. and Christie-Blick, N. (ed.). SEPM Special Publication 37: Strike-slip Deformation, Basin Formation and Sedimentation. SEPM, Tulsa, pp. 319–338. http://dx.doi.org/10.2110/pec.85.37.0319

Shi, Y.L., Cao, J.L., Ma, L. and Yin, B.J., 2007. Tele-seismic coseismic well temperature changes and their interpretation. Acta Seismologica Sinica English Edition, 20/3, 280–289. https://doi.org/10.1007/s11589-007-0280-z

Spötl, C., Plan, L. and Dublyansky, Y., 2017. Hypogene Karst in Austria. In A. Klimchouk, Palmer, A.N., de Waele, J., Auler, A.S. and Audra, P. (ed.), Hypogene Karst Regions and Caves of the World, Springer, Cham, pp. 903. https://doi.org/10.1007/978-3-319-53348-3_6

Trauth, M., 2006. MATLAB® Recipes for Earth Sciences. Springer, Berlin, pp. 237. https://doi.org/10.1007/3-540-27984-9

Wang, C.-Y., Cheng, L.H., Chin, C.V. and Yu, S.B., 2001. Coseismic hydrologic response of an alluvial fan to the 1999 Chi-Chi earthquake, Taiwan. Geology, 29/9, 831–834. https://doi.org/10.1130/0091-7613(2001)029<0831:CHROAA>2.0.CO;2

Wang, C.-Y. and Chia, Y., 2008. Mechanisms of water level changes during earthquakes: Near field versus intermediate field. Geophysical Research Letters, 35, L12402. https://doi.org/10.1029/2008GL034227

Wang, C.-Y. and Manga, M., 2010. Earthquakes and Water. Lecture Notes in Earth Sciences 114. Springer, Heidelberg, 225 pp. https://dx.doi.org/10.1007/978-3-642-00810-8

Wang, C.-Y. and Manga, M., 2015. New streams and springs after the 2014 Mw6.0 South Napa earthquake. Nature Communications, 6, 1–6. https://doi.org/10.1038/ncomms8597

Weginger, S., Jia, Y., Isaba, M. and Horn, N., 2017. Real-time Shakemap implementation in Austria. Geophysical Research Abstracts, 19, Poster, EGU2017-6624.

Wessely, G., 1983. Zur Geologie und Hydrodynamik im südlichen Wiener Becken und seiner Randzone. Mitteilungen der österreichischen geologischen Gesellschaft, 76, 27–68.

Wessely, G., 2006. Geologie der österreichischen Bundesländer – Niederösterreich. Verlag der Geologischen Bundesanstalt, Wien, pp. 416.

Wessely, G., Coric, S., Rögl, F., Draxler, I. and Zorn, I., 2007. Geologie und Paläontologie von Bad Vöslau (Niederösterreich). Jahrbuch der Geologischen Bundesanstalt, 147, 419–448.

Winkler, G., 1992. Beobachtungen an der Thermalquelle in der Eisensteinhöhle (Niederösterreich), Die Höhle, 43, 96–98.

Wyss, M. and Jackson, D.D., 1997. Cannot earthquakes be predicted? Science, 278, 487. https://doi.org/10.1126/science.278.5337.487

Zötl, J.G., 1997. The spa Deutsch-Altenburg and the hydrogeology of the Vienna basin (Austria). Environmental Geology, 29/3–4, 176–187. https://doi.org/10.1007/s002540050116

ZAMG Zentralanstalt für Meteorologie und Geodynamik, 2018. Klimadaten von Österreich 1971-2000. https://www.zamg.ac.at/fix/klima/oe71-00/klima2000/klimadaten_oesterreich_1971_frame1.htm (accessed on 25 June 2018)

8. Appendix

Appendix 1: Measurements of structural features inside Eisensteinhöhle.

ID	DipDir	Dip	DipDir2	Dip2	Sense	Comment
1	154	72				Joint, left side behind door
2	312	50				Calcite vein
3	103	34				Joint
4	134	86	64	83	/	Slickenside, no sense of shear
5	322	90	74	75	/	Slickenside, no sense of shear
6	130	85	212	86	/	Slickenside, no sense of shear
7	318	61				Calcite vein
8	309	69				Calcite vein
9	310	45				Calcite vein
10	296	68				Calcite vein
11	300	86				Calcite vein
12	285	61				Calcite vein
13	310	55				Calcite vein
14	312	76				Calcite vein
15	152	42				Calcite vein
16	300	62				Calcite vein
17	102	65				Joint

Appendix 2: MATLAB script 1 of 4. Measurements at EISE.

```
close all
clear all

%% Import Data: LEVEL_EISE 92-15
EISE9215_csv = 'EISE_level_9215.csv';
f_EISE_9215 = fopen(EISE9215_csv);
EISE_9215inp = textscan(f_EISE_9215,'%s %f','Delimiter',';');
fclose(f_EISE_9215);

date_9215_raw = datetime(EISE_9215inp{1});
level_9215_raw = EISE_9215inp{2};

clear EISE_9215file f_EISE_9215

%%  plot level_9215,  mark overflow and sampling interval >21 days
overflow = find(level_9215_raw>=307.12);
intervalgreater21days = find(days(date_9215_raw(2:end)-date_9215_raw(1:end-1))<21)+1;

figure('Name', 'Observed water level from 1992 to 2016', 'NumberTitle', 'off')
hold on
plot(date_9215_raw,level_9215_raw,'k-')
plot(date_9215_raw,level_9215_raw,'ko')
plot(date_9215_raw(overflow),level_9215_raw(overflow),'ro')
plot(date_9215_raw(intervalgreater21days),level_9215_raw(intervalgreater21days),'g.')
hold off

%% create bins and plot histogram
edges9215_start = round(min(level_9215_raw),2);
edges9215_end = round(max(level_9215_raw),2);
edges_9215 = linspace(edges9215_start,edges9215_end, (edges9215_end-edges9215_start)*10+1);

figure('Name','frequency distribution of measured water levels 92 - 16')
histogram(level_9215_raw,edges_9215)
```

```
% distribution of measurements
month_9215 = month(date_9215_raw);
y = linspace(1,12,12);
h = histcounts(month_9215);

figure('Name','Seasonal distribution of measurements and water levels')
yyaxis left
boxplot(level_9215_raw,month_9215)
yyaxis right
plot(y,h)

%% create continous 14 days interval and resample level_9015
start_date = dateshift(date_9215_raw(1),'end','month');
end_date = dateshift(date_9215_raw(end),'end','month');
duration = days(end_date-start_date)/14;
nrofSAMPLES_months = duration+1;
date = linspace(start_date,end_date,nrofSAMPLES_months);
level = interp1(date_9215_raw,level_9215_raw,date,'pchip');

save('EISE_9215', 'date', 'level')

%% IMPORT DATA: LEVEL TEMP EISE 15-17

EISE1517csv = 'Eise_1517_detail.csv';
f_EISE1517 = fopen(EISE1517csv);
EISE1517inp=textscan(f_EISE1517,'%s %f %f', 'Delimiter', ';');
fclose(f_EISE1517);

DATE_1517 = datetime(EISE1517inp{1},'InputFormat', 'dd.MM.yyyy HH:mm' );
TEMP_1517_raw = EISE1517inp{2};
LEVEL_1517 = EISE1517inp{3};
date_1517 = DATE_1517(3:end);
temp_1517_raw = TEMP_1517_raw(3:end);
level_1517_raw = LEVEL_1517(3:end);

clear f_EISE1517 EISE1517inp

% shape preserving interpolation over 1 H sample interval
date_res_1h = (linspace(date_1517(1),date_1517(end),hours(date_1517(end)-date_1517(1))+1))';
level_1517_int = interp1(date_1517,level_1517_raw,date_res_1h,'pchip');
temp_1517_int = interp1(date_1517,temp_1517_raw,date_res_1h,'pchip');

%% shape preserving interpolation over 1 day sample interval

day_min = dateshift(date_1517(1),'end','day');
day_max = dateshift(date_1517(end),'end','day');
date_res_1d = linspace(day_min,day_max,days(day_max-day_min)+1);

level_1517_int_1d = interp1(date_1517,level_1517_raw,date_res_1d,'pchip');
temp_1517_int_1d = interp1(date_1517,temp_1517_raw,date_res_1d,'pchip');

%% denoise data
level_denoise = mlptdenoise(level_1517_int,date_res_1h);
temp_denoise = mlptdenoise(temp_1517_int,date_res_1h,5);

level_denoise_1d = mlptdenoise(level_1517_int_1d,date_res_1d);
temp_denoise_1d = mlptdenoise(temp_1517_int_1d,date_res_1d);
%% Plot timeseries
%define start and end of pumping test
pumpstart1h = find(date_res_1h=='13-Jul-2016 00:00:00');
pumpstop1h = find(date_res_1h=='22-Aug-2016 00:00:00');
pumpstart1d = find(date_res_1d=='13-Jul-2016 00:00:00');
pumpstop1d = find(date_res_1d=='22-Aug-2016 00:00:00');

figure('Name','Water level and temperature changes at Eisensteinhöhle','NumberTitle','off')
yyaxis left
plot(date_res_1h,level_denoise)
yyaxis right
plot(date_res_1h,temp_denoise)
```

```
line([date_res_1h(pumpstart1h) date_res_1h(pumpstart1h)], ylim)
line([date_res_1h(pumpstop1h) date_res_1h(pumpstop1h)], ylim)

%% set pumping test nan and save for correlations, ...
EISE_date1517_1h = date_res_1h;
EISE_level1517_1h = level_denoise;
EISE_level1517_1h(pumpstart1h:pumpstop1h) = nan;
EISE_temp1517_1h = temp_denoise;
EISE_temp1517_1h(pumpstart1h:pumpstop1h) = nan;

EISE_date1517_1d = date_res_1d;
EISE_level1517_1d = level_denoise_1d;
EISE_level1517_1d(pumpstart1d:pumpstop1d) = nan;
EISE_temp1517_1d = temp_denoise_1d;
EISE_temp1517_1d(pumpstart1d:pumpstop1d) = nan;

%% histogram measurements 15-17
L_edges1 = round(min(EISE_level1517_1h),1);
L_edgesend = round(max(EISE_level1517_1h),1);
edges_L1517 = linspace(L_edges1,L_edgesend,(L_edgesend-L_edges1)*20+1);
T_edges1 = round(min(EISE_temp1517_1h),2);
T_edgesend = round(max(EISE_temp1517_1h),2);
edges_T1517 = linspace(T_edges1,T_edgesend, (T_edgesend-T_edges1)*100+1);

figure('Name','Frequency distribution of measured water level')
histogram(EISE_level1517_1d,edges_L1517)
figure('Name','Frequency distribution of measured water temperature')
histogram(EISE_temp1517_1h,edges_T1517)

%% Event summer 17

Mar17 = find(EISE_date1517_1h=='17-Mar-2017 00:00:00');
Sep17 = find(EISE_date1517_1h=='21-Sep-2017 00:00:00');

figure(7)
subplot(2,1,1)
yyaxis right
plot(EISE_date1517_1h(Mar17:Sep17),EISE_temp1517_1h(Mar17:Sep17) )
yyaxis left
plot(EISE_date1517_1h(Mar17:Sep17),EISE_level1517_1h(Mar17:Sep17))
subplot(2,1,2)

scatter(EISE_level1517_1h(Mar17:Sep17),EISE_temp1517_1h(Mar17:Sep17),'Marker','.')

%% change variable names for saving
date = EISE_date1517_1d(1:end-1);
level = EISE_level1517_1d(1:end-1);
temp = EISE_temp1517_1d(1:end-1);

save EISE_1517 date level temp
```

Appendix 3: MATLAB script 2/4. Precipitation data.

```
close all
clear variables


%% IMPORT DATA: EISE and Precipitation
EISE_1517 = load('EISE_1517.mat');
EISE_9215 = load('EISE_9215.mat');


unter = 'Unterhoeflein_92-17.txt';
f_unter = fopen(unter);
UNTERin = textscan(f_unter,'%s %f','Delimiter','\t');
fclose(f_unter);
date_UNTER_9017 = datetime(UNTERin{1},'Format','dd-MMM-yyyy','InputFormat','dd.MM.yyy HH:mm');
day_UNTER_9017 = UNTERin{2};


miesen = 'Miesenbach_90-17.txt';
f_miesen = fopen(miesen);
MIESENin = textscan(f_miesen,'%s %f','Delimiter','\t');
fclose(f_miesen);
date_MIESEN_9017 = datetime(MIESENin{1},'Format','dd-MMM-yyyy','InputFormat','dd.MM.yyy HH:mm');
day_MIESEN_9017 = MIESENin{2};


stoll = 'Stollhof_90-17.txt';
f_stoll = fopen(stoll);
STOLLin = textscan(f_stoll,'%s %f','Delimiter','\t');
fclose(f_stoll);
date_STOLL_9017 = datetime(STOLLin{1},'Format','dd-MMM-yyyy','InputFormat','dd.MM.yyy HH:mm');
day_STOLL_9017 = STOLLin{2};


sauber = 'Saubersdorf_90-17.txt';
f_sauber = fopen(sauber);
SAUBERin = textscan(f_sauber,'%s %f','Delimiter','\t');
fclose(f_sauber);
date_SAUBER_9017 = datetime(SAUBERin{1},'Format','dd-MMM-yyyy','InputFormat','dd.MM.yyy HH:mm');
day_SAUBER_9017 = SAUBERin{2};


clear SAUBER f_sauber STOLL f_stoll MIESEN f_miesen UNTER f_unter miesen unter stoll sauber


%% calculate moving sums for 14,30,90,365 days 1-365
UNTER = {};
MIESEN = {};
STOLL = {};
SAUBER = {};

for i = 1:365
    UNTER{i} = movsum(day_UNTER_9017,[i 0]);
    MIESEN{i} = movsum(day_MIESEN_9017,[i 0]);
    STOLL{i} = movsum(day_STOLL_9017,[i 0]);
    SAUBER{i} = movsum(day_SAUBER_9017,[i 0]);
end


%% resample 92-15
for i = 1:365
    unter_9215{i}=interp1(date_UNTER_9017,UNTER{i},EISE_9215.date);
    miesen_9215{i}=interp1(date_MIESEN_9017,MIESEN{i},EISE_9215.date);
    sauber_9215{i}=interp1(date_SAUBER_9017,SAUBER{i},EISE_9215.date);
    stoll_9215{i}=interp1(date_STOLL_9017,STOLL{i},EISE_9215.date);
end


%% calculate correlation coefficients and plot precipitation
% 14 day sums
[r_unt14_9215,p_unt14_9215] = corrcoef(unter_9215{14},EISE_9215.level);
[r_mies14_9215,p_mies14_9215] = corrcoef(miesen_9215{14},EISE_9215.level);
[r_stoll14_9215,p_stoll14_9215] = corrcoef(stoll_9215{14},EISE_9215.level);
[r_sau14_9215,p_sau14_9215] = corrcoef(sauber_9215{14},EISE_9215.level);


figure('Name','14-day sums of precipitation')
subplot(4,1,1)
plot(EISE_9215.date,unter_9215{14})
title(['Unterhöflein  r = ' num2str(round(r_unt14_9215(1,2),2)) ' ; p = ' num2str(round(p_unt14_9215(1,2),3)) ';'])
```

```
subplot(4,1,2)
plot(EISE_9215.date,miesen_9215{14})
title(['Miesenbach  r = ' num2str(round(r_mies14_9215(1,2),2)) ' ; p = ' num2str(round(p_mies14_9215(1,2),3)) ';'])
subplot(4,1,3)
plot(EISE_9215.date,stoll_9215{14})
title(['Stollhof  r = ' num2str(round(r_stoll14_9215(1,2),2)) ' ; p = ' num2str(round(p_stoll14_9215(1,2),3)) ';'])
subplot(4,1,4)
plot(EISE_9215.date,sauber_9215{14})
title(['Saubersdorf  r = ' num2str(round(r_sau14_9215(1,2),2)) ' ; p = ' num2str(round(p_sau14_9215(1,2),3)) ';'])

% 30 day sums
[r_unt30_9215,p_unt30_9215] = corrcoef(unter_9215{30},EISE_9215.level);
[r_mies30_9215,p_mies30_9215] = corrcoef(miesen_9215{30},EISE_9215.level);
[r_stoll30_9215,p_stoll30_9215] = corrcoef(stoll_9215{30},EISE_9215.level);
[r_sau30_9215,p_sau30_9215] = corrcoef(sauber_9215{30},EISE_9215.level);

figure('Name','30-day sums of precipitation')
subplot(4,1,1)
plot(EISE_9215.date,unter_9215{30})
title(['Unterhöflein  r = ' num2str(round(r_unt30_9215(1,2),2)) ' ; p = ' num2str(round(p_unt30_9215(1,2),3)) ';'])
subplot(4,1,2)
plot(EISE_9215.date,miesen_9215{30})
title(['Miesenbach  r = ' num2str(round(r_mies30_9215(1,2),2)) ' ; p = ' num2str(round(p_mies30_9215(1,2),3)) ';'])
subplot(4,1,3)
plot(EISE_9215.date,stoll_9215{30})
title(['Stollhof  r = ' num2str(round(r_stoll30_9215(1,2),2)) ' ; p = ' num2str(round(p_stoll30_9215(1,2),3)) ';'])
subplot(4,1,4)
plot(EISE_9215.date,sauber_9215{30})
title(['Saubersdorf  r = ' num2str(round(r_sau30_9215(1,2),2)) ' ; p = ' num2str(round(p_sau30_9215(1,2),3)) ';'])

%% 90 and 365 days
% 90 day sums
[r_unt90_9215,p_unt90_9215] = corrcoef(unter_9215{90},EISE_9215.level);
[r_mies90_9215,p_mies90_9215] = corrcoef(miesen_9215{90},EISE_9215.level);
[r_stoll90_9215,p_stoll90_9215] = corrcoef(stoll_9215{90},EISE_9215.level);
[r_sau90_9215,p_sau90_9215] = corrcoef(sauber_9215{90},EISE_9215.level);

figure('Name','90-day sums of precipitation')
subplot(4,1,1)
plot(EISE_9215.date,unter_9215{90})
title(['Unterhöflein  r = ' num2str(round(r_unt90_9215(1,2),2)) ' ; p = ' num2str(round(p_unt90_9215(1,2),3)) ';'])
subplot(4,1,2)
plot(EISE_9215.date,miesen_9215{90})
title(['Miesenbach  r = ' num2str(round(r_mies90_9215(1,2),2)) ' ; p = ' num2str(round(p_mies90_9215(1,2),3)) ';'])
subplot(4,1,3)
plot(EISE_9215.date,stoll_9215{90})
title(['Stollhof  r = ' num2str(round(r_stoll90_9215(1,2),2)) ' ; p = ' num2str(round(p_stoll90_9215(1,2),3)) ';'])
subplot(4,1,4)
plot(EISE_9215.date,sauber_9215{90})
title(['Saubersdorf  r = ' num2str(round(r_sau90_9215(1,2),2)) ' ; p = ' num2str(round(p_sau14_9215(1,2),3)) ';'])

% 365 day sums
[r_unt365_9215,p_unt365_9215] = corrcoef(unter_9215{365},EISE_9215.level);
[r_mies365_9215,p_mies365_9215] = corrcoef(miesen_9215{365},EISE_9215.level);
[r_stoll365_9215,p_stoll365_9215] = corrcoef(stoll_9215{365},EISE_9215.level);
[r_sau365_9215,p_sau365_9215] = corrcoef(sauber_9215{365},EISE_9215.level);

figure('Name','365-day sums of precipitation')
subplot(4,1,1)
plot(EISE_9215.date,unter_9215{365})
title(['Unterhöflein  r = ' num2str(round(r_unt365_9215(1,2),2)) ' ; p = ' num2str(round(p_unt365_9215(1,2),3)) ';'])
subplot(4,1,2)
plot(EISE_9215.date,miesen_9215{365})
title(['Miesenbach  r = ' num2str(round(r_mies365_9215(1,2),2)) ' ; p = ' num2str(round(p_mies365_9215(1,2),3)) ';'])
subplot(4,1,3)
plot(EISE_9215.date,stoll_9215{365})
title(['Stollhof  r = ' num2str(round(r_stoll365_9215(1,2),2)) ' ; p = ' num2str(round(p_stoll365_9215(1,2),3)) ';'])
subplot(4,1,4)
plot(EISE_9215.date,sauber_9215{365})
title(['Saubersdorf  r = ' num2str(round(r_sau365_9215(1,2),2)) ' ; p = ' num2str(round(p_sau365_9215(1,2),3)) ';'])

%% correlation of 365 precipitation sums STOLLHOF with EISE 92-15  interval 1998 - 2001
date_9801 = EISE_9215.date(177:251);
stoll_365_9801 = stoll_9215{365}(177:251);
```

```
level_9801 = EISE_9215.level(177:251);
[r_stoll9801, p_stoll9801] = corrcoef(stoll_365_9801,level_9801);


figure
subplot(1,3,[1 2])
yyaxis right
plot(date_9801,level_9801)
yyaxis left
plot(date_9801,stoll_365_9801)
title('Stollhof and EISE 1998-2001')
subplot(1,3,3)
scatter(stoll_365_9801,level_9801)
title(['r = ' num2str(round(r_stoll9801(1,2),2)) '; p = ' num2str(round(p_stoll9801(1,2),2)) ';'])


%% resample  15-17
start = find(date_STOLL_9017==datetime(EISE_1517.date(1),'Format','dd-MMM-yyyy'));
stop = date_STOLL_9017(end)
stoll_1517= {}
stoll_1517.date = date_STOLL_9017(9412:end);
stoll_1517.sum = day_STOLL_9017(9412:end);


idx_15 = find(stoll_1517.sum>=15)
% Plot EISE and stoll 15-17


[r7_stoll1517, p7_stoll1517] = movcorr(stoll_1517.sum,EISE_1517.level(1:length(stoll_1517.date)),7);
figure
subplot(2,1,1)
plot(stoll_1517.date,r7_stoll1517)
subplot(2,1,2)
plot(stoll_1517.date,p7_stoll1517)

plotregression(stoll_1517.sum,EISE_1517.level(1:length(stoll_1517.date)))


figure
yyaxis left
hold on
bar(stoll_1517.date,stoll_1517.sum)
bar(stoll_1517.date(idx_15),stoll_1517.sum(idx_15),'k')
hold off
yyaxis right
plot(EISE_1517.date,EISE_1517.level)
```

Appendix 4: MATLAB script 3 of 4. Groundwater data

```
close all
clear variables


%% IMPORT DATA: EISE and well data
EISE_1517 = load('EISE_1517.mat');
EISE_9215 = load('EISE_9215.mat');


bf1_L_tab = 'BF1_L_79-17.txt';
f_bf1_L_tab = fopen(bf1_L_tab);
BF1_L= textscan(f_bf1_L_tab,'%s %s %f','Delimiter','\t');
fclose(f_bf1_L_tab);


bf2_L_tab = 'BF2_L_76-17.txt';
f_bf2_L_tab = fopen(bf2_L_tab);
BF2_L= textscan(f_bf2_L_tab,'%s %s %f','Delimiter','\t');
fclose(f_bf2_L_tab);


br1_L_tab = 'BR1_L_70_17.txt';
f_br1_L_tab = fopen(br1_L_tab);
BR1_L= textscan(f_br1_L_tab,'%s %s %f','Delimiter','\t');
fclose(f_br1_L_tab);


%assign variables
datettime_BF1_L = strcat(BF1_L{1},',',BF1_L{2});
date_BF1_L_raw = datetime(datettime_BF1_L,'InputFormat','dd.MM.yyy,HH:mm');
datetime_BF2_L = strcat(BF2_L{1},',',BF2_L{2});
date_BF2_L_raw = datetime(datetime_BF2_L,'InputFormat','dd.MM.yyy,HH:mm');
datetime_BR1_L = strcat(BR1_L{1},',',BR1_L{2});
date_BR1_L_raw = datetime(datetime_BR1_L,'InputFormat','dd.MM.yyy,HH:mm');


lvl_BR1_raw = BR1_L{3};
lvl_BF2_raw = BF2_L{3};
lvl_BF1_raw = BF1_L{3};


% clear variables
clear f_bf1_L_tab f_bf2_L_tab f_br1_L_tab dt_BF1_L dt_BF2_L dt_BR1_L BF1_L BF2_L BR1_L


%% Period  1992 - 2015
% Crop and interpolate groundwater data 92-15
start_9215 = EISE_9215.date(1);
end_9215 = datetime('31.05.2016 00:00','InputFormat','dd.MM.yyyy HH:mm');


BF1_idx9215start = find(date_BF1_L_raw>=start_9215);
BF2_idx9215start = find(date_BF2_L_raw>=start_9215);
BR1_idx9215start = find(date_BR1_L_raw>=start_9215);


BF1_idx9215end = find(date_BF1_L_raw>=end_9215);
BF2_idx9215end = find(date_BF2_L_raw>=end_9215);
BR1_idx9215end = find(date_BR1_L_raw>=end_9215);


date_BF1_L9215 = (date_BF1_L_raw(BF1_idx9215start(1):BF1_idx9215end(1)));
date_BR1_L9215 = (date_BR1_L_raw(BR1_idx9215start(1):BR1_idx9215end(1)));
date_BF2_L9215 = (date_BF2_L_raw(BF2_idx9215start(1):BF2_idx9215end(1)));


lvl_BR19215 = lvl_BR1_raw(BR1_idx9215start(1):BR1_idx9215end(1));
lvl_BF29215 = lvl_BF2_raw(BF2_idx9215start(1):BF2_idx9215end(1));
lvl_BF19215 = lvl_BF1_raw(BF1_idx9215start(1):BF1_idx9215end(1));


level_BR1_int9215 = interp1(date_BR1_L9215,lvl_BR19215,EISE_9215.date,'pchip');
level_BF1_int9215 = interp1(date_BF1_L9215,lvl_BF19215,EISE_9215.date,'pchip');
level_BF2_int9215 = interp1(date_BF2_L9215,lvl_BF29215,EISE_9215.date,'pchip');


level_BR19215 = mlptdenoise(level_BR1_int9215,EISE_9215.date);
level_BF19215 = mlptdenoise(level_BF1_int9215,EISE_9215.date);
level_BF29215 = mlptdenoise(level_BF2_int9215,EISE_9215.date);


%% plot EISE + groundwater levels 92-15
```

```
figure('Name', 'Groundwater levels 1992-2015')
subplot(4,1,1)
plot(EISE_9215.date,level_BF19215)
title('Groundwater level at BF1')
subplot(4,1,2)
plot(EISE_9215.date,level_BF29215)
title('Groundwater level at BF2')
subplot(4,1,3)
plot(EISE_9215.date,level_BR19215)
title('Groundwater level at BR1')
subplot(4,1,4)
plot(EISE_9215.date,EISE_9215.level)
title('Water level at EISE')

%% Calculate correlation coefficients and show matrix of scatter plots

[R_BF1_G,P_BF1_G] = corrcoef(level_BF19215,EISE_9215.level);
[R_BF2_G,P_BF2_G] = corrcoef(level_BF29215,EISE_9215.level);
[R_BR1_G,P_BR1_G] = corrcoef(level_BR19215,EISE_9215.level);

[R_BF2_BF1,P_BF2_BF1] = corrcoef(level_BF29215,level_BF19215);
[R_BR1_BF1,P_BR1_BF1] = corrcoef(level_BR19215,level_BF19215);

[R_BR1_BF2,P_BR1_BF2] = corrcoef(level_BR19215,level_BF29215);

figure('Name','scatter Gerhard')
title('Scatterplots for all groundwater wells')
subplot(3,3,7)
scatter(level_BF19215,EISE_9215.level,'.')
title(['BF1/EISE  r = ' num2str(R_BF1_G(2,1)) '; p = ' num2str(P_BF1_G(2,1)) ';'])
subplot(3,3,8)
scatter(level_BF29215,EISE_9215.level,'.')
title(['BF2/EISE  r = ' num2str(R_BF2_G(2,1)) '; p = ' num2str(P_BF2_G(2,1)) ';'])
subplot(3,3,9)
scatter(level_BR19215,EISE_9215.level,'.')
title(['BR1/EISE  r = ' num2str(R_BR1_G(2,1)) '; p = ' num2str(P_BR1_G(2,1)) ';'])
subplot(3,3,5)
scatter(level_BF29215,level_BF19215,'.')
title(['BF2/BF1  r = ' num2str(R_BF2_G(2,1)) '; p = ' num2str(P_BF2_G(2,1)) ';'])
subplot(3,3,6)
scatter(level_BR19215,level_BF19215,'.')
title(['BR1/BF1  r = ' num2str(R_BR1_BF1(2,1)) '; p = ' num2str(P_BR1_BF1(2,1)) ';'])
subplot(3,3,3)
scatter(level_BR19215,level_BF29215,'.')
title(['BR1/BF2  r = ' num2str(R_BR1_BF2(2,1)) '; p = ' num2str(P_BR1_BF2(2,1)) ';'])

%% calculate corrcoef for shifted level_BF2 and level EISE
R={};
for lag=1:200
   [R{lag},P{lag}] = corrcoef(EISE_9215.level(1:end+1-lag),level_BF29215(lag:end));
   R{lag}=R{lag}(1,2);
   P{lag}=P{lag}(1,2);
end
[rmax,Imax]=max(cell2mat(R));
disp(['r max = ',num2str(rmax),' with lag of ',num2str(Imax*2),' weeks'])

% plot EISE and shifted  BF2
figure
subplot(1,3,[1 2])
yyaxis left
plot(EISE_9215.date(1:end-rmax),level_BF29215(rmax+1:end))
yyaxis right
plot(EISE_9215.date(1:end-rmax),EISE_9215.level(1:end-rmax))
subplot(1,3,3)
scatter(level_BF29215(rmax+1:end),EISE_9215.level(1:end-rmax))

%% Period  15-17

start_1517 = datetime('01.6.2015 00:00','InputFormat','dd.MM.yyyy HH:mm');
BF1_idx1517 = find(date_BF1_L_raw>=start_1517);
BF2_idx1517 = find(date_BF2_L_raw>=start_1517);
```

```
BR1_idx1517 = find(date_BR1_L_raw>=start_1517);

date_BF1_L1517 = (date_BF1_L_raw(BF1_idx1517));
date_BF2_L_false = (date_BF2_L_raw(BF2_idx1517));
date_BF2_L1517 = date_BF2_L_false(1:end-1);
date_BR1_L1517 = (date_BR1_L_raw(BR1_idx1517));
lvl_BR11517 = lvl_BR1_raw(BR1_idx1517);
lvl_BF2_false = lvl_BF2_raw(BF2_idx1517);
lvl_BF21517 = lvl_BF2_false(1:end-1);
lvl_BF11517 = lvl_BF1_raw(BF1_idx1517);

%% Interpolate and resample
% create sampling array
date_min_BF11517 = dateshift(date_BF1_L1517(1),'end','day');
date_max_BF11517 = dateshift(date_BF1_L1517(end),'start','day');
duration_BF11517 = days(date_max_BF11517-date_min_BF11517)+1;
date_res_BF11517 = linspace(date_min_BF11517,date_max_BF11517,duration_BF11517);

date_min_BF21517 = dateshift(date_BF2_L1517(1),'end','day');
date_max_BF21517 = dateshift(date_BF2_L1517(end),'start','day');
duration_BF21517 = days(date_max_BF21517-date_min_BF21517)+1;
date_res_BF21517 = linspace(date_min_BF21517,date_max_BF21517,duration_BF21517);

date_min_BR11517 = dateshift(date_BR1_L1517(1),'end','day');
date_max_BR11517 = dateshift(date_BR1_L1517(end),'start','day');
duration_BR11517 = days(date_max_BR11517-date_min_BR11517)+1;
date_res_BR11517 = linspace(date_min_BR11517,date_max_BR11517,duration_BR11517);

level_BR1_int1517 = interp1(date_BR1_L1517,lvl_BR11517,date_res_BR11517,'pchip');
level_BF1_int1517 = interp1(date_BF1_L1517,lvl_BF11517,date_res_BF11517,'pchip');
level_BF2_int1517 = interp1(date_BF2_L1517,lvl_BF21517,date_res_BF21517,'pchip');

level_BR11517 = mlptdenoise(level_BR1_int1517,date_res_BR11517);
level_BF11517 = mlptdenoise(level_BF1_int1517,date_res_BF11517);
level_BF21517 = mlptdenoise(level_BF2_int1517,date_res_BF21517);

%%
figure
subplot(3,1,1)
plot(EISE_1517.date,EISE_1517.level)
title('EISE')
subplot(3,1,2)
plot(date_res_BF21517,level_BF21517,date_res_BF11517,level_BF11517)
title('BF1 blue / BF2 red')
subplot(3,1,3)
plot(date_res_BR11517,level_BR11517)
title('BR1')

%% interpolate over pumping test and crop BF2 for correlation

level_BF21517_int = interp1(date_res_BF21517,level_BF21517,EISE_1517.date,'linear');
EISE_1517.levelint = interp1(EISE_1517.date,EISE_1517.level,EISE_1517.date,'pchip');

figure
yyaxis left
plot(EISE_1517.date,EISE_1517.levelint)
yyaxis right
plot(EISE_1517.date,level_BF21517_int)

[r_BF2, p_BF2] = corrcoef(EISE_1517.levelint(~isnan(level_BF21517_int)),level_BF21517_int(~isnan(level_BF21517_int)));
disp(r_BF2(1,2))
```

Appendix 5: MATLAB script 4 of 4. Earthquake catalogue

```
clear variables
close all
clc

%% IMPORT DATA: EISE_1517 and Austrian Earthquake Catalogue

EISE_1517 = load('EISE_1517.mat');

erdbebencsv = 'AEC_9217.csv';
f_ERD = fopen(erdbebencsv);
EQin= textscan(f_ERD,'%s %s %f %f %f %f %s %s %f %f %f %f %f %f %f %f %f %f %f %s','delimiter',';');
fclose(f_ERD);
date = strcat(EQin{1},{' '},EQin{2});
date_ind = find(date>=EISE_1517.date(1));

EQ_1517 = {};
EQ_1517.date = datetime(date(date_ind),'InputFormat','dd.MM.yyyy HH:mm:ss');
EQ_1517.depth = EQin{5}(date_ind);
EQ_1517.magnitude = EQin{6}(date_ind);
EQ_1517.Location = EQin{7}(date_ind);
EQ_1517.epi_distance = EQin{12}(date_ind);
EQ_1517.hypo_distance = EQin{13}(date_ind);
EQ_1517.pgv = EQin{15}(date_ind);
EQ_1517.pga = EQin{16}(date_ind);
EQ_1517.epi_proximity = EQin{18}(date_ind);
EQ_1517.hypoc_proximity = EQin{19}(date_ind);
clear EQin f_ERD

pgv_01_idx = find(EQ_1517.pgv>0.1);
pgv_250_idx = find(EQ_1517.pgv>250);
M_Dkm_str =strcat('M =  ',num2str(EQ_1517.magnitude),'; ',num2str(EQ_1517.epi_distance),' km');

figure
yyaxis left
plot(EISE_1517.date,EISE_1517.level)
yyaxis right
hold on
stem(EQ_1517.date(pgv_01_idx),EQ_1517.pgv(pgv_01_idx),'Marker','none')
for k=pgv_250_idx(1:end)
%     txt=[num2str(EQ_1517.epi_distance(i));
    text(EQ_1517.date(k),EQ_1517.pgv(k),M_Dkm_str(k,:))
end
hold off
```